coatings

MDPI

Review

Nanocrystalline Cermet Coatings for Erosion–Corrosion Protection

Abhishek Tiwari [1,*], Saravanan Seman [1,2], Gaurav Singh [1] and Rengaswamy Jayaganthan [1,*]

[1] Department of Engineering Design, Indian Institute of Technology Madras, Chennai 600036, India; saravana.met@gmail.com (S.S.); pankaj.gaurav.singh@gmail.com (G.S.)
[2] Department of Metallurgical and Materials Engineering, IIT Madras, Chennai, Tamil Nadu 600036, India
* Correspondence: abhishektiwariiitr@gmail.com (A.T.); edjay@iitm.ac.in (R.J.); Tel.: +91-4422574735 (R.J.)

Received: 3 May 2019; Accepted: 6 June 2019; Published: 20 June 2019

Abstract: The processing techniques, microstructural characteristics, and erosion corrosion behaviour of Cr_3C_2–NiCr and tungsten carbide (WC)-based cermet coatings are reviewed in this work. Conventional and nanocrystalline Cr_3C_2–NiCr and WC-based cermet coatings are generally synthesized using thermal spray technique. The wear, erosion, and corrosion protection ability of conventional and nanocermet coatings are compared based on available literature. In Cr_3C_2–NiCr coatings, the corrosion resistance is offered by NiCr metal matrix while the wear resistance is provided by the carbide ceramic phase, making it suitable for erosion–corrosion protection. The nanocrystalline cermet coatings exhibits better erosion–corrosion resistance as compared to the conventional coatings. The nanocrystalline coatings reduces the erosion–corrosion rate significantly compared to conventional coatings. It is attributed to the presence of the protective NiCr metallic binder that allows easier and faster re-passivation when the coating is subjected to wear and the fine-grain structure with homogeneous distribution of the skeleton network of hard carbide phases. In addition, corrosion-accelerated erosion dominates the reaction mechanism of erosion–corrosion and, therefore, higher hardness, strength, and better wear resistance of nanocermet coating along with its faster repassivation kinetics accounts for improved corrosion resistance as compared to conventional coatings.

Keywords: thermal spray; Cr_3C_2-NiCr; erosion–corrosion; wear; nanocrystalline

1. Introduction

A material is designed according to its specific application and exposure to environment. Some environments may be very aggressive, such as offshore oil and gas production plants where both erosion and corrosion of components could occur. In hydro power turbine industries, equipment like pumps, impellers, and turbine blades are exposed to aggressive conditions. Slurry erosion, abrasive wear, erosive wear, cavitation erosion, and erosion–corrosion are the main causes for material degradation in hydro power turbine system [1]. Therefore, design of material is critical to avoid premature failures due to erosion–corrosion and resulting costs and replacement of equipments [2]. Erosive wear results in removal of material through deformation and cutting actions caused by impact of solids, liquids, gases, or the combination of these [3]. The erosion–corrosion in principal is mechanical erosion of the material or oxide layer on its surface and enhanced corrosion of the material as, generally, the corrosion rate is governed by thickness of oxide layer on material surface. Corrosion and its mitigation continue to cost roughly 4% of GDP of any developed economy, which translates to billions of dollars to the world economy [4]. A traditional approach to solve such an erosion–corrosion problem is by increasing chromium contents of engineering alloys as it forms a protective oxide film. However, such oxide films can be disrupted easily when subjected to erosive corrosive environments.

Corrosion mitigation approaches include plating, cathodic protection, and hexavalent chromium Cr (VI). However, chromium (VI) is considered toxic and, therefore, environmental friendly coatings are necessary [5]. Prasanna et al. [3] studied the role of high-velocity oxy-fuel (HVOF) coatings to combat erosion in turbine alloys. The super alloys used for high-temperature application such as solar thermal power plants, heat exchangers, gas, and steam turbines suffer from the drawback of poor creep and erosion–corrosion resistance at high temperatures. To obviate this problem, protective coatings are deposited on super alloys. Coatings provide erosion–corrosion resistance whereas the super alloys fulfil the structural integrity of components with required strength at elevated temperatures [3]. Cr_3C_2–NiCr coating deposited through thermal spray coating has emerged as one of the best corrosion protective coatings to combat erosion and wear loss of the materials used in hydro power turbines. In this coating, chromium carbide particles are embedded in a NiCr metallic matrix [6]. HVOF-sprayed tungsten carbide (WC) coating also offers remarkable erosion resistance shield to combat low- and high-energy particle impingement wear, making such coatings suitable when subjected to corrosive erosive environments in hydropower plants severely affected due to silt particles [7]. The HVOF process thermal spray technique uses kinetic energy of the burnt gases for softening and propelling the spray powder producing dense, very low porosity, good inter-particle cohesion, and well-bonded coatings with high hardness values [3,8]. Stellite-6, 10% Al_2O_3 + 90% CoCrAlTaY and 25% Cr_3C_2-20(Ni-Cr) + 75% NiCrAlY were sprayed on three kinds of turbine alloys, namely Ti-6Al-4V, Co-based super alloy (Super co 605), and Fe-based special steel (MDNI21) [3]. Such coatings are used for applications in rocket motors, structural forgings and fasteners, pressure vessels, gas turbine blades, and furnace equipment [3]. The powders used for coatings are chosen such that they offer resistance to hot corrosion and erosion [3]. HVOF spraying uses a supersonic jet created by the burning of liquid petroleum gas and oxygen gas [3]. Cr_3C_2-25(Ni20Cr) + NiCrAlY coating shows behavior of both brittle and ductile materials. The brittle erosion deals with material removal due to crack formation and high porosity of coatings, where silica particles are implanted into open porosity [3]. The increase in porosity of coatings appears to display less impact on the erosion of the material [3]. Thermally sprayed Cr_3C_2–NiCr coatings on 310S Steel when subjected to high-temperature corrosion in molten salt (Na_2SO_4-60% V_2O_5) at 700 °C offers hot corrosion resistance as compared to bare 310S, due to the formation of oxide layers such as Cr_2O_3 and $NiCr_2O_4$, and follow parabolic rate law for corrosion [9]. Cr_3C_2-NiCr coatings provide better hot corrosion resistance compared to NiCrAlY + 0.4 wt% CeO_2 and NiCoCrAlYTa coatings because of partial oxidation of NiCrAlY + 0.4 wt. % CeO_2 and NiCoCrAlYTa coatings and ash deposition [10]. The MCrAlY (M = Ni and/or Co) coatings have been used for corrosion protection of superalloy components in high-temperature environments such as gas turbines [11,12]. Rana et al. demonstrated that NiCrAlY coating provided desired hot corrosion resistance in air and molten salt (Na_2SO_4-60% V_2O_5) due to formation of slow-growing Al_2O_3 in the oxide scale, and coatings deposited using flame spray technique offered better hot corrosion resistance compared to those deposited by high-velocity oxy-fuel (HVOF) sprayed technique [13,14]. The choice of Na_2SO_4-60% V_2O_5 is to simulate actual boiler conditions developed inside a steam generator due to burning of low-grade fuels [13].

Hong et al. [15] have reported that WC-10Co-4Cr coating exhibits comparable microbial-influenced corrosion resistance in seawater with sulfate-reducing bacteria (SRB) as compared to the stainless steel (1Cr18Ni9Ti) using potentiodynamic polarization and electrochemical impedance spectroscopy studies (EIS). Parida et al. [16] demonstrated that Ni-based plasma spray coatings provide satisfactory means of producing acceptable sealing surface with excellent abradability. Bobzin et al. [17] investigated tribological properties of Cr_3C_2–NiCr coating and observed that the thick HVOF-sprayed coatings do not undergo adhesive failure when the load acting upon it is less than 1000 N.

Thermal spraying is a suitable technique for forming a hard nanocrystalline coating due to the fact that its particle melting, rapid cooling, and consolidation in a single-step operation results in low porosity, higher bond strength, and increased wear properties. Nanocrystalline coatings with grain sizes in the nanometer range are driven by the improvement in coating technologies attributable to

significant improvement in the properties, and the various kinds of synthesized nanopowders can be used as feedstock materials for thermal spray processes such as plasma spraying, HVOF spraying, detonation flame spraying, flame spraying, wire arc spraying, etc. HVOF is suitable compared to other techniques to deposit dense nanocrystalline cermet coatings because of its higher droplet velocity and lower thermal energy levels, yielding denser structure, and higher bond strength between the coating and the substrate. Uniform distribution of carbide phase in metal matrix, decrease of the interconnected porosity, and a lower roughness in the nanostructured coating are responsible for better performance in corrosion, wear, and erosion–corrosion tests in 0.6 wt. % NaCl solution [6]. Electrochemical data suggested that the corrosion rate of conventional chromium coatings is increased compared to nanostructured coating by almost one order of magnitude by the mechanical damage [6]. WC-Co-based nanostructured coating has provided better protection of the substrate from corrosion due to its nobler behavior and enhanced sealing properties, which is attributed to its lower porosity. Electrochemical measurements in 80 mL of an aerated and un-stirred 3.4% NaCl solution and salt fog spray test (with a 5% NaCl solution at 35 °C, 15 mm^3/h of collected solution, and 1 bar) results of nanostructured coating show 350% increase in corrosion resistance compared with conventional coating [18].

Nanostructured WC-10Co4Cr coating showed low erosion wear compared to conventional coatings due to higher microhardness value, lower porosity, higher fracture toughness, and lower roughness, and these are attributed to the size of the powder particles (200–500 nm), the density of the coating, and the more uniform distribution of reinforcement carbides (WC) [19]. Nanostructured Ni-20Cr coating was found to perform better than its conventional coatings in a boiler environment due to the presence of protective film and oxide phases; furthermore, cyclic formation and erosion of the oxide scales occurred during erosion–corrosion phenomenon for coated samples as compared to steel substrate, which was most likely eroded [20]. Conventional WC-12Co coatings have lower erosion–corrosion resistance compared to nanostructured coating, and a corrosion-enhanced erosion mechanism dominates the erosion corrosion process in 3.5 wt. % NaCl solution with 13.3% silica sand (500 μm) [21]. The surface morphology of the conventional coating was rough and the number of pits and their size (~40 μm) were larger than those for the nanostructured WC-12Co coating (~20 μm) [21].

The present review is focused mainly on conventional and nanocrystalline Cr_3C_2–NiCr and WC-based cermet coatings fabricated by thermal spray technique and their erosion-corrosion behaviors corroborated by detailed investigations reported in the literature so far.

2. Cr_3C_2-NiCr and WC-Based Cermet Coatings

Cr_3C_2-NiCr and WC-based cermet coatings obtained by thermal spraying technique with conventional grains show excellent wear and corrosion resistance, but the microstructure of such thermally sprayed coatings are found to be inhomogeneous with discontinuities like pores, oxide lamellas, or incomplete molten spray particles [6,7,22]. Such discontinuities are detrimental to material strength and performance. To reduce such inhomogeneity, researchers have developed nano-structured cermet coatings with lower porosity and high surface quality. However, thermal spraying of such nano-structured coating slurries is a problem for feeding particles <10 μm when compared to conventional coarse-grained powders [6,23].

By definition, erosion-corrosion is the accelerated degradation of a material under combined effect of mechanical erosion and electrochemical attack, both of which assist each other during the process of degradation. As a combination, this effect is called the synergy effect, which causes higher material loss to that of combined effects of individual erosive and corrosive actions. With respect to synergy, combined effects can be explained as removal of protective film via erosion, which leads the exposed surface for further corrosion and removal of work hardened surfaces from material via corrosion, which expose the underlying bare metal for further erosion.

$$\text{Total loss } (T) = \text{loss due to corrosion } (C) + \text{loss due to erosion } (E) + \text{synergy effect } (S)$$

Thus,

$$S = T - (C + E).$$

Synergy can be broken down in to two components, ΔE_c and ΔC_E, where ΔE_c is the corrosion-enhanced erosion and ΔC_E is the erosion-enhanced corrosion [2].

Among Cr_3C_2-NiCr and WC-based cermet coating systems, Cr_3C_2-NiCr is the most prominent erosion–corrosion-resistant coating [2,23].

2.1. Thermal Spray Techniques for Synthesis of Cr_3C_2-NiCr and WC-Based Cermet Coatings

Thermal spray coatings have been developed and employed as an alternative to hard layer deposition techniques involving deposition of a hard metal alloy layer over a metal substrate, which shows better protection under abrasion compared to normal heat-treated steel but are not applicable to all shapes and also increase the weight of the final component. Therefore, a superior method available for applying metallic coatings is thermal spray technique, which has been used widely in industrial applications. There are various types of thermal spray techniques available, such as detonation-gun (D-gun), plasma spraying, and HVOF spraying technique. Semi-molten or molten powders are deposited at a high speed onto a substrate to produce a 2D coating using the HVOF technique. The microstructure and properties of the coating depend on various spraying parameters and types of feedstock materials. Feedstock materials can be in the form of rod, wire, or powders. Such coatings are characterized qualitatively through phase stability, adhesive strength, hardness, toughness, oxide contents, and surface roughness. There are numerous applications of thermal spray, some of which are thermal barrier coatings, wear-resistant coatings, and corrosion-resistant coatings [24–26].

HVOF process is a type of thermal spray process introduced by Browning and Witfield in the early 1980s [26]. HVOF utilized a combination of oxygen with fuel gases like hydrogen, propane, propylene, or kerosene. The mixture obtained is, thus, introduced into a combustion chamber where combustion takes place and produces a high-temperatue and high-pressure supersonic gas flowing through a nozzle. The powder particles introduced into this jet and these particles fully or partially melt during the flight until it reaches the substrate, where melting depends on the flame temperature, particle dwell time, material melting point, and thermal conductivity of material [26]. The flame temperature varies between 2500 to 3200 °C, depending on the fuel type and ratios of fuel and oxygen in the mixture [26]. HVOF thermal spraying technique has been proved successful in developing the high-quality cermet coating, especially for materials with melting point below 3000 °C, with the use of a hot combustion supersonic stream-driven high-velocity gas jet (e.g., 700–900 ms^{-1}), since it shows advantages in density and bond strength as a higher amount of fine carbides embedded in it makes it attractive for wear and corrosion resistance applications [27–33]. HVOF thermal spray coatings have environmental advantages as compared to chemically/electrochemically formed coatings [7]. The HVOF process has an ability to produce dense coatings with less degradation and oxidation of metallic materials, while also retaining primary phases. The reason behind this is the small dwell time of particle flight and relatively cold flame. However, the drawback of this technique is that coatings produced are not 100% crystalline [26]. The benefits of HVOF include higher gas velocity, lower porosity, and better cohesion compared to plasma spray, wire arc spray, and wire flame spray techniques [8,26].

Appropriate use of suspension compositions in suspension thermal spraying (SPS) is an important factor for nanocrystalline cermet coatings. Conventional methods cannot be used for nano particles due to their lower mass relative to conventional powders. The nano particles can decompose quickly owing to the high thermal energy imparted as a result of their smaller size. The atmosphere of thermal spraying can lead to carbon loss in high-temperature environments compared to micro conventional powders. The variation in particle size leads to uneven distribution, which can be resolved by employing a suspension feed system and carefully controlling the coating process parameters. HVOF with use of suspensions allows axial injection directly into the burning chamber and this can be combined with the water-based suspensions having high solids content for nanocrystalline cermet coatings [34]. The important variables for the formation of nanosized crystals in thermal-sprayed

coatings are the size of crystals in initial feedstock, method of spraying, and temperature of substrate at coating, which may influence the nucleation of crystals. Low temperature would promote formation of fine grains but results in a bad thermal contact between splats and substrate and high temperature results in a good thermal contact between splats and substrate resulting in a greater cooling rate of the splats [35]. The suspension plasma spraying (SPS) and high-velocity suspension flame spraying (HVSFS or S-HVOF) techniques are mostly used for suspension spraying in terms of particle temperature and velocity [35,36]. Suspension-sprayed coatings, which allow the direct injection of nanosized to submicron-sized powders, thus avoiding the necessity of powder agglomeration with the water and alcohols as a transport media, can result in either nanocomposite coating or a bimodal coating [37–39]. The S-HVOF process with nanostructured feedstock powder can lead to nanostructured and amorphous phases in the microstructure of the coating as compared to conventional HVOF. The microstructure of the S-HVOF processed WC-Co coating contains nanosized particles (WC, W, M_6C, $M_{12}C$) with particle sizes in the range of 100–300 nm [40]. Lower value of friction coefficient and higher sliding wear resistance are observed in S-HVOF as compared to the conventional HVOF coatings [40].

2.2. Chracterisation of Cr_3C_2-NiCr and WC-Based Cermet Coatings

Cr_3C_2-NiCr and WC-based cermet coatings are generally characterised using SEM and EDS (energy dispersive spectroscopy), X-ray diffraction (XRD), and transmission electron microscopy (TEM) techniques to ascertain crystallinity, microstructure morphology, and different phases present in the coating. Typical images of coatings are shown in Figure 1.

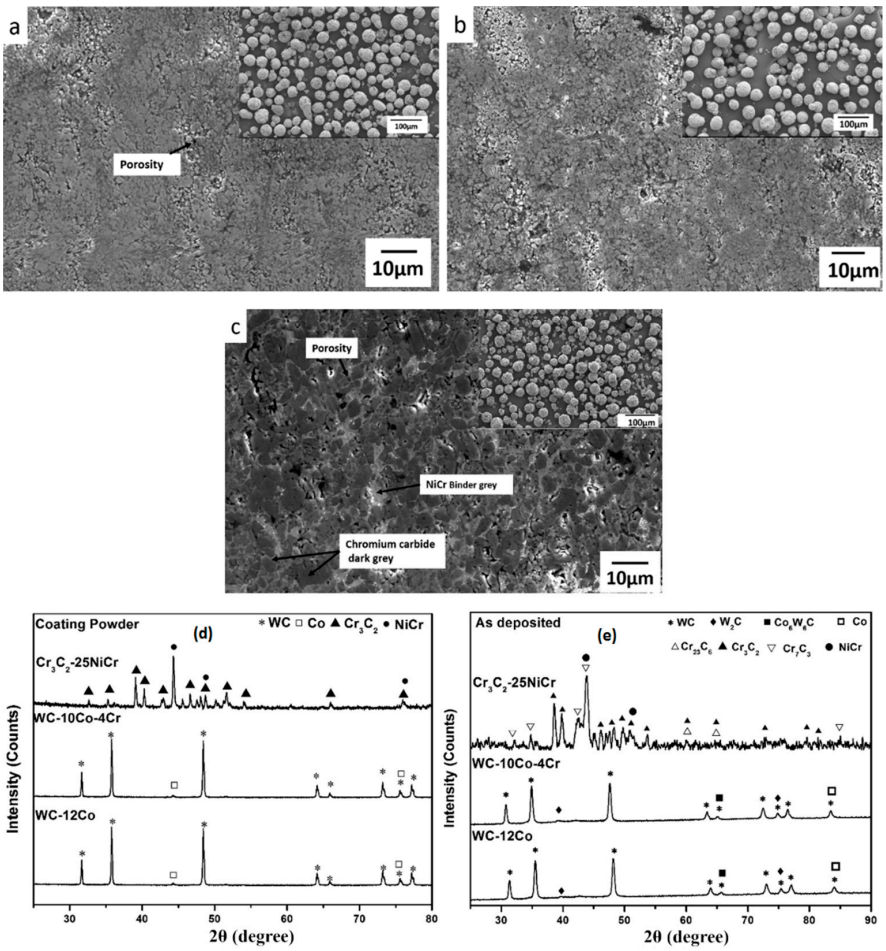

Figure 1. SEM micrographs of the coatings (**a**) WC-12Co, (**b**) WC-10Co-4Cr, and (**c**) Cr_3C_2–NiCr and XRD patterns of (**d**) initial feedstock powders and (**e**) as sprayed coatings. In the inset, SEM images of feedstock powders are shown [41]. Reprinted with permission from ref [41]. © 2017 Elsevier.

Spherical shape of Cr_3C_2–25NiCr powder reveals more porous features compared to WC–12Co and WC–10Co–4Cr feedstock powders as shown in Figure 1a–c, and carbide particles are aggregated with metallic binder. Bright and dark regions are indicative of the metallic binder phase and the carbide phase, respectively. The presence of WC and Co phases in tungsten carbide coating and Cr_3C_2 and NiCr in Cr_3C_2-NiCr are confirmed by XRD patterns (Figure 1d,e). Moreover, in WC-based coatings, a strong peak of WC with a minor peak of W_2C and Co_6W_6C, and in Cr_3C_2–NiCr coating, NiCr, Cr_3C_2, Cr_7C_3, and $Cr_{23}C_6$ peaks are observed in Figure 1 [41].

During HVOF spraying, the splat deposited directly on the substrate is subjected to a cooling rate from 106 to 108 K s^{-1}, which allows the NiCr binder phase to solidify in the form of an amorphous phase at the area adjacent to the coating/substrate [33]. NiCr matrix is found to be a fine-grain structure along with large grain size in the region far away from the interface due to variation in the cooling rate. In the Cr_3C_2–NiCr coating, besides Cr_3C_2 particles retained from the starting powder, the carbides Cr_7C_3, and $Cr_{23}C_6$ are also present and these carbides are formed through decarburization of Cr_3C_2 [33].

2.3. Nanostructured Cermet Coatings

The microstructre of coatings with ultrafine grains/particles exhibit technologically important structural and functional properties. The nanocrystalline coatings offer high strength and toughness and high thermal resistance with lower thermal conductivity. Despite several bottlenecks in synthesizing such nanocrystalline coatings, they are very attractive due to their applications [42–44]. In nano-structured coating systems, components utilize a plurality of relatively hard, brittle nano-sized particles disposed within a relatively ductile matrix and methods of manufacturing HVOF process providing enhanced wear and erosion resistance at both high and low temperatures [45].

The nanocrystalline coatings are characterized by average grain size less than 100 nm [46]. In the case of nanocrystalline grain size, more than 50% of atoms are associated with grain boundaries due to small grain size resulting in more contribution towards physical properties of material [25]. Nanocrystalline coatings can be deposited using several techniques, yet thermal spraying has been reported by several researchers as one of the best techniques available [46–55]. Thermal spraying with nanostructured feedstock powders has resulted in higher hardness, strength, and corrosion resistance compared to conventional powders. This improved strength of nano-phased materials is due to the fact that they are nearly dislocation-free, and dislocations are known for lowering strength and hardness of metals/alloys. Also, the fine size of nano particles give them a large specific surface area, which leads to high activity, and nano particles can be melted easily and evenly with severe deformation compared to the conventional micro-grained coatings, which experience surface melting only (Figure 2).

Thermal spraying proves to be a very effective and economic process. An advantage of using thermal spraying in depositing nanocrystalline coating is that the aggregation of such powders does not affect the spray process, which, in the case of micro-crystalline coatings, could have a negative effect [25,56–58].

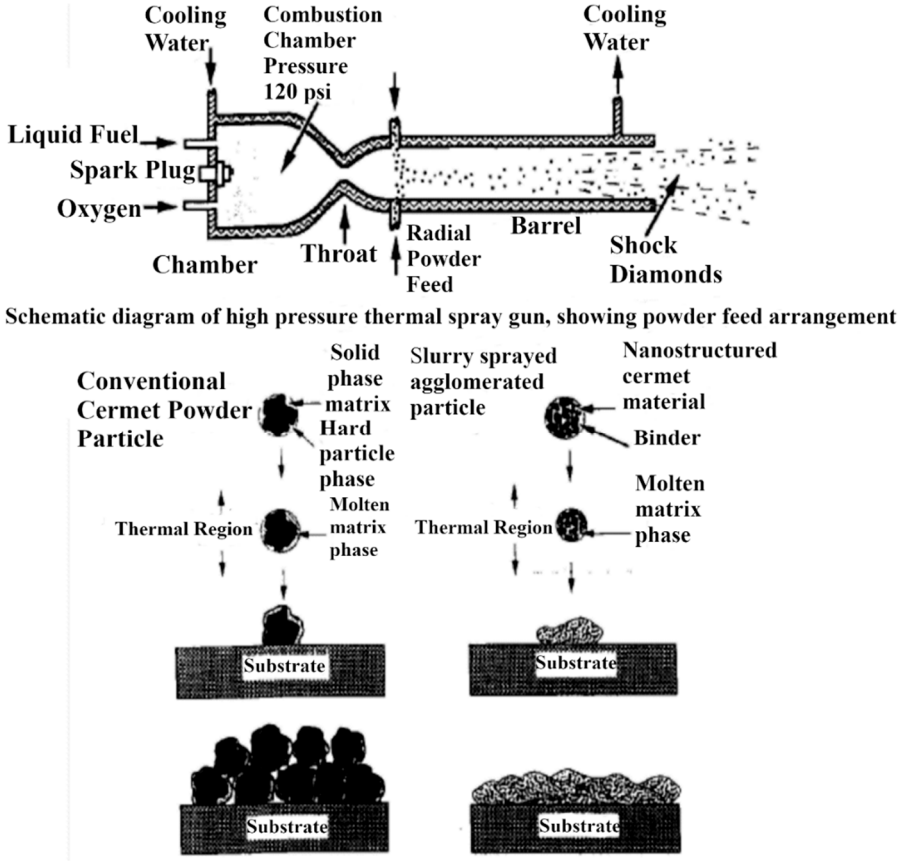

Figure 2. Comparison between thermal spraying of conventional and nanostructured powders [42]. Reprinted with permission from ref [42]. © 1995 Elsevier.

2.3.1. Synthesis of Nanocrystalline Feedstock Powders

There are numerous techniques available for producing nanostructured material such as thermochemical method, mechanical alloying/milling, vapor deposition, condensation, spray conversion processing, crystallization of amorphous alloys, sputtering, electro-deposition, and sol-gel processing techniques [25].

The two most important methods are discussed here:

(a) **Chemical processing:** In general, for industrial application, chromium carbide cermet powders are synthesized by crushing, grinding, blending, and consolidation of the constituent powders. The limitation of this method is that the scale of the morphological and compositional variation is determined by size of the phases in the blended powder; also, during processing, it is prone to include impurities, whereas the advanced thermochemical method uses precursor compounds in which respective elements A, B, and C are mixed at molecular level [59]. A, B, and C compounds are made using aqueous solution and transferred into nanostructured AC/B followed by thermochemical conversion. The first step involved spray drying of aqueous solution containing appropriate quantities of Cr, Ni, and C to synthesize Cr_3C_2/Ni cermet as the end product [59]. Spray-dried precursor powder is heated at >1100 °C in a tube furnace for 5 h in an inert gas environment [59]. This heat treatment allows solid-state chemical reactions resulting in conversion of spray-dried powder to nanostructured form [59]. Peter et al. [60] patented aqueous solution reaction (ASR) and organic solution reaction (OSR) methods for producing nanostructured Cr-C/NiCr and WC/Co powders in the form of loose agglomerates of variable size and morphology. Using these procedures, powders can be ultrasonically dispersed in an aqueous or organic liquid medium with a polymer or paraffin binder and spray dried to form uniform-sized spherical agglomerates of 5–25 μm diameter. Moreover, during thermal spraying,

the nano-composite powders experience partial melting and undergo splat quenching when they impact the substrate surface [60].

(b) **Mechanical alloying/milling:** This method is used to produce a large quantity of nanostructured material. This method can also be employed to produce a variety of compositions. There are four types of mills available to carry out milling: (1) Attritor mill, (2) uniball mill, (3) vibratory mill, and (4) planetary mill. Among them, attritor mill has the highest charge capacity. It utilizes a stainless-steel container with several horizontal impellers joined to a rotating (around 180 rpm) vertical shaft driven by external motor [25]. It consists of a ball-to-powder-mass ratio of 20:1 [25,61]. Rotating impellers energize the moving balls, which further causes grain size refinement of powder by impact under a controlled milling environment. A controlled environment is necessary to decrease contamination of powder and control powder temperature. The milling environment can be gaseous, liquid, or solid. In some cases, using a liquid environment like liquid nitrogen, methanol, acetone, etc., can affect powder particle size and morphology [25]. Xu [62] reported that the embedded sub-particle or plurality of embedded sub-particles may include various metal, carbon, metal oxide, metal nitride, metal carbide, intermetallic compounds, or cermet particles, or a combination thereof by any suitable method, including, for example, by ball milling or cryo-milling hard particles together with the particle core material.

2.3.2. Thermal Spraying of Nanocrystalline Coatings

Nanostructured coatings using thermal spray can be formed, either by starting with nanostructured powders or creating nanostructures during the spraying process. Usually, it starts with a nanostructured feedstock powder of suitable size as required by HVOF spraying. Mechanical alloying (MA) technique is used as it can produce a sufficient quantity of nanostructured powder with good reproducibility under varying compositions. There are various parameters that influence the formation of intermetallics during mechanical alloying such as type of milling, time, and temperature of milling [24,25]. The average particle size of Cr_3C_2–25NiCr decreases to a value of 5 μm with increasing milling time, whereas in Inconel 625, particle size increases to 84 μm and a significant change is seen within the first 4 h of milling in both cases [24,25]. Lavernia [63] proposed a two-step approach for producing nanocrystalline coatings. First, the grain size of micrometer-sized powders is reduced to nanometer size using high-energy ball milling (attritor mills). Second, the nanocrystalline powders are dried, agglomerated, and sprayed by HVOF process to produce a coating with refined microstructure.

Some degree of melting is always required for a sufficient level of particle adhesion and cohesion over the substrate. But in the case of nano-structured agglomerated feedstock particles, it is necessary to avoid full melting during thermal spraying in order to preserve the nanostructure. In such coatings, it is likely that semi-molten feedstock particles will spread throughout the coating microstructure surrounded by fully molten particles that act as a binder, to maintain coating integrity. An important issue related to fine/nano particles smaller than 100 nm is that they cannot be thermally sprayed using the currently available regular powder feeders, as these tiny nano-particles clog the hoses and fittings placed in between powder feeder and thermal spray torch [64]. In order to inject individual nanoparticles into a spray jet, a high carrier gas flow is required, which can destabilize the thermal spray jet and affect the penetration level of individual nanoparticles into the substrate's layer, making the deposition process very inefficient. Therefore, nano-sized particles are agglomerated into microscopic particles via spray-drying [64,65].

2.3.3. Characterization of Nano-Crystalline Powder Synthesized by Mechanical Milling

Powder characteristics such as particle size, powder morphology, grain size, phase constituents, and deformation faults are very important from the point of view of producing an effective nanostructured coating. The Cr–C system can be found in three crystallographic structures or intermetallic compound forms: cubic $Cr_{23}C_6$, hexagonal Cr_7C_3, and orthorhombic Cr_3C_2, where the last one has the highest melting point. These can be synthesized from chromium and carbon

mixtures via high-energy milling or mechanical alloying. The powder particles are subjected to severe mechanical deformation during high-energy ball milling, where they are repeatedly deformed, cold welded, fractured, and re-welded. Initially, Cr clusters are destroyed in the milling process and the fine particles are formed, which are further reduced with increasing milling time [6,25,66–71].

Cr_3C_2-based cermet powders, when deposited using the HVOF spray technique, result in a very thin coating within a surface roughness region and do not require a grinding process. Surface roughness mainly depends on the maximum particle size of the sprayed powder and will be approximately 10% of the diameter of the largest powder particle [6]. The microstructure of such a coating usually consists three regions: One that retains the initial nanostructure (grey), another with a larger spherical hard phase (dark grey) embedded in binder (bright), and the last one is a bright band, attributed to the nickel-based binder. Previous literature has shown that in nanostructured Cr_3C_2–NiCr coatings, the presence of an amorphous matrix phase is not identified clearly, which is observed in a conventional HVOF thermally sprayed Cr_3C_2–NiCr coating [66]. In nanostructured Cr_3C_2–NiCr coatings, few discontinuous elongated amorphous phase forms as HVOF spraying process undergo a temperature of 2400 K, which is sufficient to melt the NiCr binder matrix completely (melting point 1700 K) and these molten matrix regions are rendered amorphous during impingement and rapid cooling with the surface commonly known as splat-quenching [66]. When these nanostructured coatings are heat treated at 1073 K, some very fine precipitates are formed by nucleation and growth in the matrix in addition to original carbide particles. Also, the average size of the original carbide particles increases in the range of 24–39 nm, whereas the precipitates are formed of an average size of 8.3 nm [25,66,72].

Another important aspect comes from TEM investigations, which show a slight growth in grain size of the coating applied using HVOF thermal spray when utilizing high-energy milled metallic materials. The difference in temperature attained by particles during flight cause a wide range of grain size distribution. Such a microstructure formed during spraying is dependent on powder particle size and morphology, which influence the melting conditions during spraying. Thus, it requires a uniform particle size distribution to compare grain growth between coatings based on precursor powders [42].

Further, it has been seen that if nanostructured agglomerated ceramic powders are utilized to form thermal spray coatings, they exhibit a bimodal microstructure, consisting of fully molten in addition to semi-molten particles. The semi-molten particles (i.e., nano-zones) can be dense or porous. During thermal spraying, a dense nano-zone occur when the molten part of a semi-molten particle fully or almost fully infiltrates into the capillaries of the agglomerates, whereas in the case of limited infiltration, porous nano-zone are formed (Figure 3) [64].

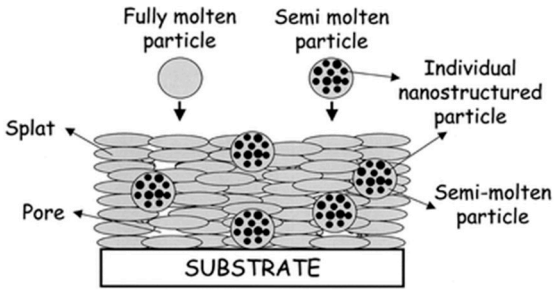

Figure 3. Typical schematic of the bimodal microstructure of thermal spray coatings formed by fully molten and semi-molten nanostructured agglomerated particles [64]. Reprinted with permission from ref [64]. © 2007 Springer Nature.

Gomari and Sharafi demonstrated that angular-shaped Cr powders, when mixed with irregular-shaped C powders using ball milling under inert gas atmosphere, led to cold welding of powders. It is found in their study that between 2 h and 6 h of ball milling, agglomerations were changed and primary Cr clusters were destroyed and their size began to decrease with an increase in

milling time (Figure 4) [70]. These particles led to fracture after 6 h of milling, and a steady state was achieved after 10 h of milling [70].

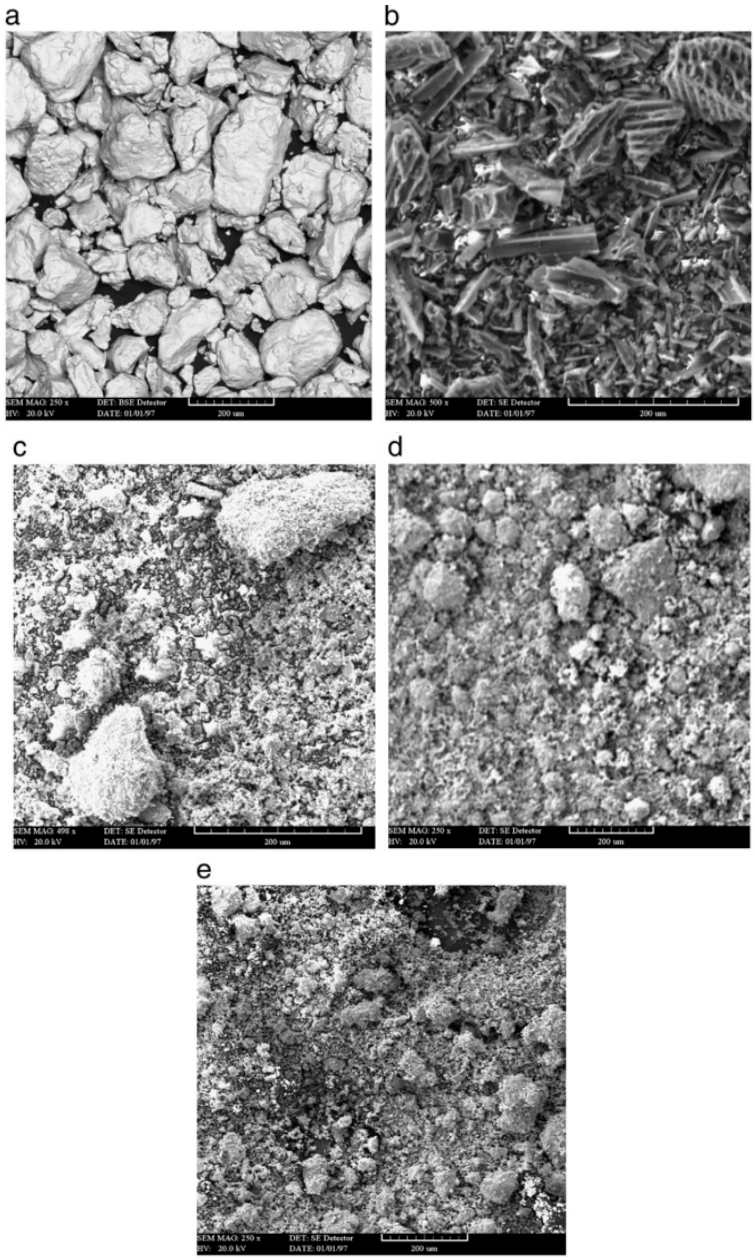

Figure 4. SEM micrographs of (**a**) chromium powders, (**b**) carbon powders, (**c**) Cr_3C_2 mixture milled for 2 h, (**d**) Cr_3C_2 mixture milled for 6 h, and (**e**) Cr_3C_2 mixture milled for 10 h [70]. Reprinted with permission from ref [70]. © 2012 Elsevier.

The milling mechanism for Cr_3C_2–NiCr cermet/composite powder consists of a hard and brittle carbide particle constituent and a tough metal binder constituent. During milling, these carbide particles are fractured into sharp fragments and embedded into the metal binder. Carbide fragments continue to embed into the metal binder with increasing milling time. The metal binder and the polycrystal composite experience continuous overlapping, cold welding, and fracturing, and these sharp carbide fragments in the polycrystal composite are shaped into round particles. Finally, a polycrystal nanocomposite powder system with uniformly distributed round nano-scale carbide particles in a metal binder is formed [25].

3. Wear Resistance of Cr_3C_2-NiCr and WC-Based Nanostructured Coatings

Hardness of a material is a parameter that is always associated with wear resistance. Wear rate of cermet coatings depends on morphology of powder, the size, shape, and distribution of the carbide particles, hardness of the carbide particles relative to the abrasive media, properties of matrix and its volume portion, and the coating method, which governs the characteristics of coating like the phases, density, micro and macro hardness, and residual stresses [73]. The characteristics and performances of the resulting coatings are strongly influenced by the presence of defects, which corresponds to partly and fully melted particles with oxides, cracks, and porosity, as well as residual stresses [73]. In the case of Cr_3C_2-NiCr cermet coatings, it has been reported in the literature that hardness value increases from 846 HV to 1020 HV (20.5% increase) when shifting from microstructured coatings to nanostructured coatings [74,75]. This increased hardness is due to the uniformity of microstructure and presence of nano-phases and this high hardness is, to some extent, contributed to by high kinetic energy and low thermal energy associated with the HVOF process. Further, with the increase in temperature (or coating under heat treatment), the micro-hardness of the conventional coating increases slightly, whereas in the case of nanostructured coating, this increase is a significant 1020–1240 HV [75]. Another important aspect is that the coating with conventional grains shows a lower coefficient of friction compared to coating with nano-crystalline grains. Also, the work hardening rate of nano-crystalline grain is high due to restricted deformation of nano-scale grains, which inhibit dislocation activity, or due to high volume fraction of the grain boundary present. Heat treatment of nanostructured Cr_3C_2-NiCr coatings also increases the scratch resistance and decreases the coefficient of friction (half of the value obtained at ambient temperature), which can be explained by the presence of high density of Cr_2O_3 oxide particles with average size of 8.3 nm in the nanostructured coatings exposed to high temperatures [75]. Micro-hardness of a material depends on its microstructure, size, distribution, and behavior of the precipitates formed and usually affects hardening. High density of fine, hard, and dispersed precipitates in the matrix significantly increases micro-hardness [24,56,66,75–78].

Two distinct varieties of pores can be seen in the nanostructured coatings: (i) Those that are striated and can be as large as 10 μm (due to pulling out of carbide particles), and (ii) those that are much smaller, less than 1 μm, and distributed uniformly. The large difference between abrasive particles' size and hard phase particles' size influences the wear resistance of the nanostructured coatings, resulting in less protection of the binder phase. However, in nanostructured coatings, high wear resistance is resulted by compensating the lower protection by hard phase particles to that of higher hardness in the nanostructured precursor powders. If abrasives causing wear are in the submicron range, then the small hard phases in nanostructured coatings might be more protective than micrometer-sized hard phases present in conventional coatings [56,72]. Tetyana et al. [79] discovered that the thermally sprayed coatings with an amorphous-nanocrystalline-microcrystalline composition structure exhibit enhanced wear resistance, corrosion resistance, and thermal stability than conventional coatings.

Mechanical and wear behavior of the reported coatings are summarized in Table 1. In Cr_3C_2–NiCr and WC-based coatings using the HVOF thermal spray technique, low porosity of cermet coatings can be achieved due to fast deposition rates, which results in good wear resistance, oxidation resistance, and adhesion properties [8,17,21,22,41,47,80–86].

Table 1. Mechanical and wear behavior of the reported coatings.

Process	Coating	Particle Size (μm)	Porosity (%)	Thickness (μm)	Micro-hardness	Roughness (R_a)	Fracture Toughness (MPa $m^{1/2}$)	Elastic Modulus (GPa)	Specific Wear Coefficient k, (mm^3/Nm)	Friction Coefficient	Ref.
HVOF	Cr_3C_2–20(80Ni20Cr) WC–Ni	−45 + 10 −45 + 15	-	221 ± 16 118 ± 8	982 ± 35 ($HV_{0.1}$) 977 ± 82 ($HV_{0.1}$)	2.74 ± 0.31 4.71 ± 0.44	4.40 ± 0.31 3.06 ± 0.86	-	-	-	[87]
HVOF	Cr_3C_2–25NiCr	-	1–2	500–590	614–810 ($HV_{0.3}$)	-	-	-	-	-	[80]
CAPS	Cr_3C_2–25NiCr	-	-	84.1–155.2	290.7–609.1 ($HV_{0.3}$)	6.75–10.83	-	-	5.72×10^{-7}–2.29×10^{-7}	0.48–0.718	[88]
HVOF	WC–17Co WC–12Co WC–10Co4Cr Cr_3C_2–40NiCr Cr_3C_2–25NiCr	20–40	-	100–200	1024 ($HV_{0.3}$) 1038 1154 855 918	3.7–4.9	2.6 - 2.4 3.7 3.5	-	-	-	[89]
HVOF	Conventional WC–12Co Nanostructured WC–12Co CeO_2-modified WC–12Co	15–45 5–45 15–45	0.60 ± 0.04 0.52 ± 0.04 0.35 ± 0.03	-	10.6 ± 0.3 (GPa) 12.2 ± 0.4 12.2 ± 0.4	-	4.0 ± 0.3 5.5 ± 0.4 5.2 ± 0.4	119.6 ± 9.3 226.9 ± 18.7 204.1 ± 17.1	-	-	[21]
HVOF	WC–CoCr Cr_3C_2–NiCr Al_2O_3	−45 + 15 −45 + 15 −22 + 5	0.240 1.306 1.347	163 176 294	1364 (HV) 1006 1164	4.119 1.855 1.063	-	-	-	-	[81]
HVOF	Cr_3C_2–25NiCr	−45 + 15	-	250	780 ± 116 (HV)	<0.1		380	2×10^{-7} (100 h at 400 °C)	0.65–0.55	[90]
HVAF HVOF	Cr_3C_2–25NiCr	−38/+10 −45/+15	4–6	300–400	1021 ± 110 ($HV_{0.1}$) 919 ± 161	-	3.62 ± 0.35 4.13 ± 0.33	185.5 ± 1.5 170.7 ± 1.9	5×10^{-6} (at 400 °C) 1×10^{-5} (RT)	0.70–0.75(RT) 0.05 (at 400 °C)	[47]
HVOF	Cr_3C_2–25NiCr WC-10Co–4Cr	−45/+15 −45/+15	1.56 2	225 221	~800 (HV) ~1000	3.35 6.51	-	-	-	-	[82]
HVOF	Cr_3C_2–25NiCr Cr_3C_2–WC–NiCoCrMo	−45/+15	1.4 ± 0.1 1.1 ± 0.1	-	1029 ± 94 ($HV_{0.3}$) 1153 ± 42	-	-	-	33.3 ± 1.6–37.2 ± 2.1 × 10^{-6} (450–650 °C) 6.3 ± 0.5–11.5 ± 0.3 × 10^{-6}	(450–650 °C) 0.474 ± 0.034–0.427 ± 0.032 0.574 ± 0.038–0.481 ± 0.041	[83]
HVOF	WC–12Co WC–10Co–4Cr Cr_3C_2–25NiCr	−45/+15	1.2 1.1 1.5	350	1270 ± 100 ($HV_{0.3}$) 1148 ± 100 825 ± 80	5.23 5.28 6.18	4.5 ± 1.0 5.1 ± 0.7 3.7 ± 0.9	-	-	-	[41]
HVAF HVOF	WC–10Cr–4Co	−45/+16 −30/+5	0.52 ± 0.13 0.98 ± 0.3	380–420	1473 ± 40 ($HV_{0.3}$) 1180 ± 70	2.28–4.48	5.60 ± 0.15 3.86 ± 0.7	-	-	-	[84]
APS	Cr3C2–NiCr Ni–Cr–Fe	10–90	-	200 150	0.239 (GPa) 0.217	-	-	22.795 23.375	-	0.515 1.298	[91]
HVOF	WC–12Co WC–12Co–10Al_2O_3 WC–12Co–15Al_2O_3	WC-12Co: 24 ± 5 Al_2O_3: 10 ± 5	-	255 ± 5	950 ± 50 (HK) 1200 ± 50 1300 ± 50	5.93 5.41 5.44	-	-	2.99×10^{-5} 5.26×10^{-6} 3.19×10^{-6}	0.8 0.5 0.7	[85]
HVOF	Cr_3C_2–25NiCr	−45/+15	<1	260–280	949 ± 83 ($HV_{0.1}$)	0.70	-	205 ± 17	-	-	[17]
HVOF	Cr_3C_2–20NiCr	-	<1.8	325	902 (HV)	5.206	-	-	-	-	[86]
HVOF	WC/Co coating: Multimodal M1 Multimodal M2 Conventional coarse grained Ultrafine grained Nanocrystalline	 WC/12Co: (WC/Co: 2–3, WC: ~30 nm) WC/10Co: (WC/Co: 2–3, WC: ~30 nm) - 0.2–0.3 0.03–0.05	-	-	 1100 820 1080 1150 1150	-	-	-	 5.3×10^{-6} 6.7×10^{-6} 4.5×10^{-6} 3.7×10^{-6} 3.7×10^{-6}	-	[92]
HVOF	Commercial WC–12Co Nanostructured WC–12Co	−45/+5.5 Agglomerated: 40 Carbide particle: 6 ± 3 (nm)	-	-	1129 ± 50 ($HV_{0.3}$) 1135 ± 50	-	-	-	-	-	[93]
HVOF	WC–18Co	20 32 38	-	100	1004 ($HV_{0.1}$) 825 735	-	-	-	0.28×10^{-6} 0.32×10^{-6} 0.30×10^{-6}	-	[94]

Note: HVOF—high-velocity oxy-fuel; HVAF—high-velocity air-fuel; CAPS—controlled atmospheric plasma spray; APS—atmospheric plasma spray.

High hardness of HVOF coating among all coatings is attributed to a high velocity of the injected feedstock powder particle which impart more kinetic energy leading to better densification, homogeneous microstructure with uniform distribution of hard particle, reduced interconnected porosity and metal binder oxidation. Moreover, HVOF coating offers good bond strength and lower degree of decarburization due to low temperature and high kinetic energy. Cr_3C_2–25NiCr powder particles, having lower melting point, allowed powder to result in strong bonding with the substrate compared to relatively less melted or un-melted WC based powder particles which led to less rough surface and low porosity of Cr_3C_2–25NiCr coating. No significant pores and microcracks present in the interface of the coating. The nanostructured HVOF WC based coating exhibits the highest microhardness, elastic modulus, and fracture toughness due to the uniform distribution of the carbide particles in the matrix. The lower hardness and surface roughness of Cr_3C_2–25NiCr compared to WC based coating was attributed to the relatively higher concentration of NiCr softer binder phase. HVOF coating shows superior wear resistance, which is attributed to higher hardness and less porosity. Furthermore, the phase transformation, decomposition, and decarburization of the carbide particles can influence wear behavior of the coatings. WC-based coatings exhibited high hardness and wear resistance as compared to Cr_3C_2–NiCr coatings due to the presence of hard WC particles embedded in the matrix or binder phase. Although WC-based coatings are harder and more wear resistant than Cr_3C_2-based coatings, their operating temperature is limited to less than 450 °C; however, Cr_3C_2-based coatings are utilized in corrosive and moderate wear environment at the temperature up to 850 °C. During abrasion, the formation of the tribo oxide film with low shear strength, which became stable and resistant against delamination up to 850 °C was responsible for the reduction in friction coefficient of Cr_3C_2–NiCr coating and also their greater fracture toughness reduces cracking during surface grinding and tribocorrosion tests [41,47,82,83,87,89,92]. The volume fraction of Cr_3C_2/Ni-Cr matrix has an influence on the surface roughness of the coating and when its volume fraction increases from 0.24 to 2.14, average roughness value is reported to increase by ~42% [88]. Heat-treated Cr_3C_2–25NiCr coatings exhibited the significant effect of aging temperature on hardness and the initial drop of hardness observed (780 ± 116 HV) was due to the release of the residual stresses, which can significantly modify the spallation resistance (resistance to surface failure in which spall is shed), thermal cycling, and fatigue properties. Further increasing the annealing time results in microstructural modifications, leading to the significant increase in hardness about 950 HV for the most severe condition (100 h at 400 °C). In this aging condition, the wear rate was about 2×10^{-7} $mm^3/(N{\cdot}m)$, showing a value about 80% lower than that obtained in the as-coated condition. Moreover, the improved tribological resistance of the aged Cr_3C_2–25NiCr coatings results from the high hardness and from the formation of stable and protective oxides during previous aging [90]. Dry particle abrasion involves coarse abrasive grooving and pull-out of coating fragments, which are closely related to the mechanical properties reflecting long-range inter-lamellar cohesion (such as fracture toughness and elastic modulus), and partly related to microhardness, which depends on intra-lamellar cohesion. Furthermore, sliding wear involves shallower abrasive grooving, carbide pull-outs, and limited adhesive wear contributions. Sliding wear at room temperature bears some relation to hardness, however the mechanisms occurred at the intra-lamellar level. Meanwhile, the fine feedstock powder provides slightly more wear-resistant coatings than the coarse one, due to a stronger matrix-carbide cohesion inside the lamellae after spraying. Although the numerous carbide grains are responsible for sliding wear, the amount of defects in the carbide grains and their cohesion to the matrix controls the sliding wear, too [47].

The effect of heat treatment and role of microstructure in the erosion mechanism of Cr_3C_2-NiCr thermal spray coatings have been discussed in detail by research group of Steven Matthews from University of Auckland [95–97]. In their work, it was observed that as-sprayed Cr_3C_2-NiCr coatings were subjected to temperatures in the range of 700–900 °C, and the Cr diffused from carbide phase to NiCr phase, which led to Cr concentration to the point that it allowed Cr_2O_3 formation to dominate from earliest exposure times. The ductility of the NiCr phase is found to be increased due to heat treatment of as-sprayed Cr_3C_2-NiCr coatings, resulting in ductile deformation features during erosion

without brittle interphase cracking and improved inter-splat cohesion from sintering. The mechanism of impact response of Cr_3C_2-NiCr coatings is found to be dependent upon the depth of erodent penetration [97]. Matthew et al. [98] investigated the variation in microhardness of HVOF thermal spray 75Cr_3C_2–25NiCr coatings subjected to 900 °C for 60 days in air and Ar atmosphere as a function of microstructural evolution. It was found in their study that super-saturation of the matrix phase was decreased, while carbide nucleation growth produced an expansive carbide skeletal network. Due to heat treatment, first, softening of the coating occurred through matrix phase refinement, then hardness was recovered as a function of carbide development. Therefore, precipitation of fine carbides and their growth resulted in microstructural changes leading to changes in hardness values. The heat treatment of the samples in air has increased hardness due to internal oxidation. Further, Matthew et al. [99] subjected Cr_3C_2-NiCr coatings to 900 °C for 30 days and tested them for erosion corrosion at ambient and elevated temperature. In the as-sprayed HVOF and HVAF Cr_3C_2-NiCr coating, deformation occurred via brittle cracking and fracture of the matrix phase at ambient temperature. The coating splat structure was found to be a preferential path for crack propagation in HVOF coating but was insignificant in the case of HVAF coating. The ductility of as-sprayed coatings has shown improvement in erosion at 800 °C. The in-flight degradation of coatings reduced the carbide concentration. The heat treatment in general was found to improve matrix ductility and toughness, reducing the brittle matrix response. Carbide precipitation due to heat treatment has formed an extensive network, which provided resistance towards erosion during impact and thereby enabled the applied load to be distributed over the entire microstructure. The same research group has also demonstrated relative erosion corrosion rate of Cr_3C_2–NiCr coatings at 700 and 800 °C under impact velocity of 225–235 m/s under a simulated turbine environment [100]. The HVOF and HVAF sprayed coatings produced almost similar erosion rates in both as-sprayed and heat-treated coatings, which is attributed to complex transition under the influence of brittle matrix phase in the case of as-sprayed coating and influence of carbide network in case of the heat-treated coating. The erosion rate of heat-treated coating has increased due to constraints upon the matrix by carbide network.

Uniform distribution and stronger grain strengthening of WC fine particles with nanostructured grain size result in smoother surface, higher hardness, elastic modulus, fracture toughness, and better wear resistance, along with strength of a material of the nanostructured WC-Co coating. Fine nano powder particles reached higher temperature and produced harder coatings, which results in high hardness and low porosity compared to larger particles. The nanostructured WC-Co coating showed better sliding wear behavior and the higher microhardness. Moreover, friction coefficient was 30% lower than that of the conventional coating. Though nanostructured WC-Co coatings have intrinsically refined microstructures obtained through optimized thermal spray parameters, reported high hardness value of 1135 HV is not achieved because of higher surface area per unit volume and the temperature of nano powder in the material causing severe decarburization/decomposition of WC carbide [18,21,92–94].

Compared to conventional coatings, agglomeration of fine nano particles are required as a feedstock material for the nanostructured HVOF spraying process to produce nanostructured cermet coatings, which results in high mechanical and wear properties due to low porosity with dense, hard, and uniform distribution of the microstructure of the coatings, because detrimental flowability of nano particles causes improper coating during spraying. The nanocrystalline particle melts with relative ease, leading to high density and low porosity with unmelted or partially melted coarse particles embedded within the matrix. The coatings with such structures are likely to be hard, ductile, and wear resistant, and heat treatment of the nanostructured coating may also enhance the mechanical properties, wear, erosion, and corrosion behavior [21,47,83,90,92–94].

4. Erosion–Corrosion Resistance of Cr_3C_2-NiCr and WC-Based Nanostructured Coatings

Erosion–corrosion behavior of carbide-based cermet coatings is well known and has been studied separately by many researchers. However, the combined effect of erosion (wear) and corrosion holds

great interest among scientists as such situations arise quite regularly in many industrial applications. There are various parameters that can affect the electrochemical behavior of coated samples, some of which include localized corrosion attack, removal of coating through wear causing unprotected surface exposure, accumulation of corrosive product on the surface causing wear action, etc. It is also observable that weight loss by summation of separate losses associated with wear and corrosion is lower than the weight loss obtained under combined action of both [64]. Erosion-corrosion of Cr_3C_2-NiCr coatings is dependent on carbide/metal matrix proportion [101]. It was observed that the cermet coatings were eroded by SiO_2 quartz and fly ash at a low velocity with peak wastage at an intermediate value of carbide content for both the shallow and steep angles [101]. Erosion caused by the bed ash at a high velocity showed no peak wastage at either the shallow or the steep angles [101]. Instead, the erosion-corrosion thickness loss increased with the increase in NiCr metal binder content [101].

Fedrizzi et al. utilized a setup, shown in Figure 5, for tribo-corrosion test, where he used electrochemical impedance measurements to obtain polarization resistance trends during tribo-corrosion [6]. Tribo-corrosion tests were carried under free immersion, applying an anodic current and, finally, lubricated wear test under cathodic protection. Surface degradation due to combined wear and corrosion damage was also measured by calculation of samples' weight loss after the tests [6]. The weight loss measurements after corrosion or tribo-corrosion test were carried out in the following ways, in order to find out the relative importance of wear and corrosion on total degradation:

1. Wear-corrosion test at open circuit potential (0.6 wt. % NaCl solution) using 200 rpm rotation/5 N applied load;
2. Corrosion test at open circuit potential in the same electrolyte without any applied load;
3. Lubricated wear test was obtained in the same electrolyte using 200 rpm rotation speed and 5 N applied load.

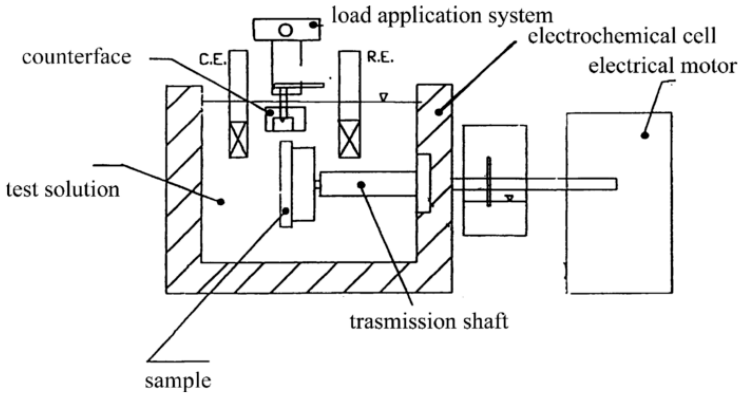

Figure 5. Sketch of the apparatus used for tribo-corrosion tests [6]. Reprinted with permission from ref. [6]. © 2004 Elsevier.

Experiments by Fedrizzi et al. have shown that nanostructured coatings show better performance under simple corrosion, simple wear, as well as in a combined action of both erosion and corrosion, due to a well-distributed chromium carbide phase in metal matrix, and also due to low porosity and lower roughness of nanostructured coatings [6]. Figure 6 shows a comparison between micro-sized and nano-sized coatings in terms of volume loss, which shows that nano-powder coatings display a remarkably smaller volume loss with respect to the conventional coatings under all the selected working conditions. Synergistic effect has been confirmed by weight loss measurement results. It can be seen in electrochemical data that mechanical damage enhances the corrosion rate of these coatings. Also, the presence of a large amount of ceramic particles in the composite coating made the corrosion a less important phenomenon in overall degradation [6].

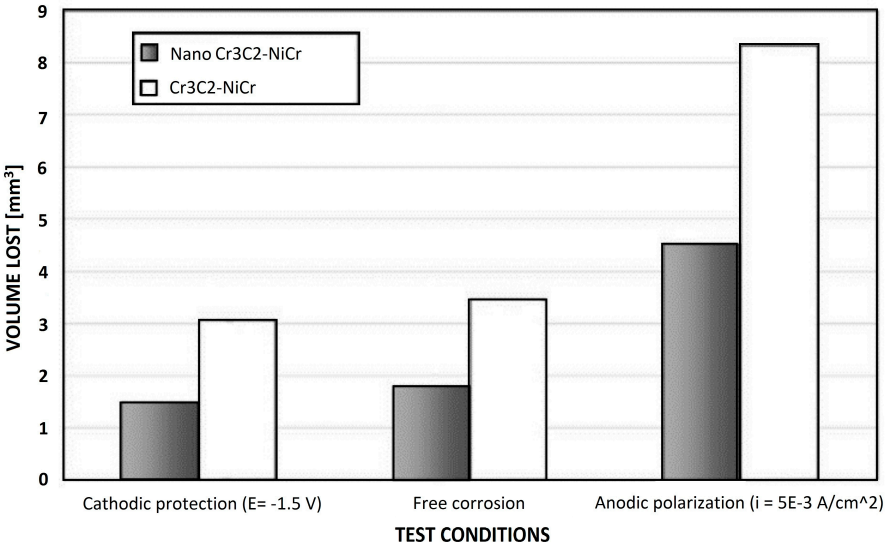

Figure 6. Volume loss of the high-velocity oxy-fuel (HVOF) coatings under the different tribo-corrosion conditions [6]. Reprinted with permission from ref [6]. © 2004 Elsevier.

Potentiodynamic polarisation studies showed that Cr_3C_2-NiCr and hard chromium coatings showed decrease in corrosion current and increase in E_{corr} [102]. Both decrease in corrosion current and positive shift in E_{corr} are indicative of corrosion protection ability of a coating. Therefore, it may be inferred that the 480 mV positive shift in E_{corr} in the case of the Cr_3C_2-NiCr-coated sample in the potentiodynamic polarization curve and the 130 mV positive shift for the hard coatings show the corrosion protection ability of both the coatings, with the former coating demonstrating better corrosion resistance (Figure 7) [102].

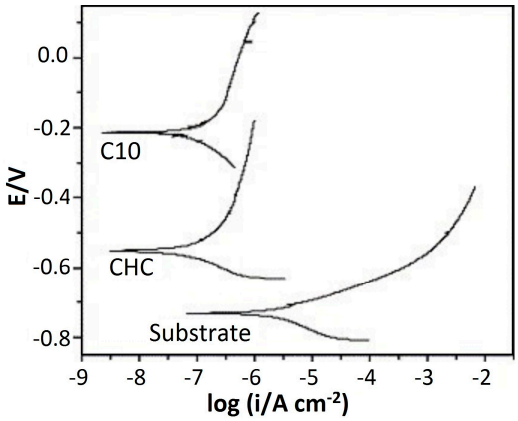

Figure 7. Potentiodynamic polarization curves for C10 (Cr_3C_2–NiCr-coated sample), CHC (hard chromium coating), and steel substrate after 20 h immersion in 3.4% NaCl at 25 °C [102]. Reprinted with permission from ref [102]. © 2006 Elsevier.

Further, EIS studies exhibited that both hard chromium and Cr_3C_2–NiCr coatings showed high corrosion resistance for short immersion times. However, the time dependent EIS studies showed that the corrosion resistance of Cr_3C_2–NiCr coatings decreases with time. The corrosion resistance of hard chromium coating has revealed only small variations with time [102].

Erosion and corrosion behavior of the reported coatings is summarized in Table 2. The HVOF spraying process is the preferred process of depositing Cr_3C_2–NiCr cermet coatings as it exhibits high density, low porosity, as well as excellent adhesive strength, and numerous carbide particles remain in the matrix compared to the plasma spraying process [17,73,103–106]. Porosity or voids and surface roughness are the important parameters contributing to higher erosion or corrosion resistance

of the Cr_3C_2–NiCr coating [86]. WC-based thermal-sprayed coatings can provide superior erosion and corrosion resistance compared to various substrate materials due to low porosity and better microstructure with superior cohesiveness of the splats lamellae, and uniform distribution of the carbide particles together attributed to higher hardness and denser and minimal decarburized WC phase in the microstructure [107]. However, Chakradhar et al. reported that the addition of Al_2O_3 showed higher I_{corr} values than those of bare stainless steel, which indicates that HVOF coatings have poor corrosion resistance, due to the porous nature of the coatings [15,21,49,84,85,108,109]. The erosion–corrosion mechanism of the WC-based HVOF coatings is first dominated by erosion of the binder phase prior to the corrosion, causing brittle detachment of hard phase due to mechanical effect. In addition to the erodent particle and impact angle, velocity can also influence the erosion–corrosion behavior of the coatings [49,84,108,109]. The erosion-wear mechanism of the WC–CoCr coating is micro-cutting, and plowing at a low angle and rounding of the edges of the WC grains leads to brittle cracking at a higher angle, whereas in slurry-erosion, the mechanism of the coating is cracking and micro chipping in distilled water together with detachment of binder phase, microchipping, and fragments in 3.5 wt. % NaCl slurry [15,84]. Compared to Cr_3C_2–NiCr coating, the room temperature oblique (30°) impact erosion resistance of WC–10Co–4Cr coating was poor because of higher porosity, which offered a number of sites for penetration by high-speed erodent particles to remove chunks of material. In addition, WC grains knockout easily from the lower proportion of Co metal matrix from WC-based coating; furthermore, a higher proportion of Cr in the matrix of Cr_3C_2–NiCr coating has shown improved wear and oxidation resistance [82]. The splat and globular morphology offers high density of the Cr_3C_2–NiCr coating in addition to formation of Cr_2O_3 and spinel of Ni and Cr, which can enhance the degradation resistance, and calculated parabolic constant value during oxidation is found to be one-third of the substrate, which shows the superior oxidation resistance. Furthermore, both polarization and EIS results confirmed that the corrosion protection properties of the HVOF coating were superior to the substrate as well as the plasma coating due to the formation of less pores on the top surface during the test [103–105]. Though the erosion mechanism of Cr_3C_2–NiCr coating was ductile and brittle, the ductile mode of erosion characteristic dominates. During erosion, small crater volumes were generated initially under impact loading, plastic deformation, tribo-reaction, along with micro-abrasion, however the crater volume increases rapidly when high forces start due to high velocity of the erodent [17,106].

Table 2. Erosion and corrosion behavior of the various cermet coatings.

Process	Coating	Substrate	Test Method	Main Findings	Ref.
HVOF Arc spray Plasma spray Flame spray Flame spray Plasma spray	Cr_3C_2–25NiCr FeCrSiB Ni base Cr_3C_2–6SiO–4Al_2O_3 Cr_3C_2–12SiO–2Al_2O_3–4MgO WC–NiCrCo	1018 steel	Erosion test	HVOF Cr_3C_2–NiCr coating offers better erosion–corrosion resistance compared to those of 1018 steel and of other cermet and ceramic coatings due to its compactness, high density, fine grain structure. and a homogeneous distribution of the skeletal network of hard carbide/oxide within a ductile and corrosion-resistant metallic binder.	[110]
HVOF	Ni–Cr–Si–B–C	Austenitic stainless steel (UNS S31603)	Weight loss test Potentiodynamic anodic polarization test	The cermet coating was found to be better than the stainless steel in material loss during solid–liquid conditions. During solid-free impingement, greater material loss was observed, and this was attributed to the relative influences of erosion and corrosion.	[48]
HVOF Flame spray Plasma spray	WC–Cr_3C_2–NiCr Cr_3C_2–NiCr WC–Co WC–Co–Cr Cr_3C_2–Al_2O_3–TiO_2 Cr_3O_2	High alloyed 1.4571 steel	Erosion corrosion test (0.1 M NaOH and 0.1 M H_2SO_4) Electrochemical polarization measurements and salt spray test	WC–Co coating showed the least resistant among the other coatings. WC–based coating exhibits the improved erosion and corrosion resistance by the addition of 4 wt. % Cr. HVOF-sprayed Cr_3C_2–NiCr coating is considered to be an excellent replacement for the thermal sprayed Cr_3C_2 coatings due to its low erosion and corrosion rate.	[111]
Super D-Gun thermal Spray	WC–Co–Cr	Stainless steels (UNS S31603 and UNS S32760)	Erosion–corrosion impingement test Electrochemical analysis DC anodic polarization test	Compared with stainless-steel WC–Co–Cr thermal-sprayed coatings offered good protection against wear and corrosion in liquid–solid impingement. Coating damage is controlled by erosion processes and is more important at the lower solid levels. Corrosion is affected by erosion processes at lower solid levels.	[108]
HVOF	WC/Co–Cr	Mild steel	Erosion–corrosion impingement test Electrochemical analysis	Erosion–corrosion regimes for the substrate and the coating are affected by the impact velocity and applied voltage. Interaction of mechanical and electrochemical processes are responsible for degradation of the coating.	[49]
HVOF	WC83–Co17, WC88–Co12 WC86–Co10Cr4 Cr_3C_2–40NiCr Cr_3C_2–25NiCr	C45 steel substrates	Potentiodynamic polarization test Tribocorrosion test	Cr_3C_2–NiCr coatings showed good barrier protection compared to other coatings. Chemical composition of the Cr_3C_2–NiCr coating and nickel–chromium matrix allows easier and faster re passivation even though coating is subject to wear.	[89]
HVOF	Cr_3C_2–NiCr WC–Ni	UNS-G41350 steel	Erosion–corrosion test Electrochemical analysis Electrochemical Impedance Spectroscopy (EIS) and Potentiodynamic polarization test	At high erosive conditions, WC–Ni coatings exhibited the lowest material loss and high erosion–corrosion resistance compared to chromium carbide and hard chromium coatings due to its as high hardness. Cr_3C_2–NiCr coatings showed the best corrosion performance under lower erosive-corrosive conditions compared to hard chromium coatings. Electrochemical measurements showed that Cr_3C_2–NiCr coatings showed the superior corrosion resistance compared to WC–Ni under both erosive conditions by electrochemical measurements.	[87]
HVOF	WC–10Co–4Cr	Stainless steel 1Cr18Ni9Ti	Cavitation-erosion (CE) test	The coating exhibited higher cavitation–corrosion resistance than that of the stainless-steel 1Cr18Ni9Ti in 3.5 wt. % NaCl solution The removal mechanism for the coating was erosion of the binder phase first, followed by brittle detachment of hard phases as a result of the action of corrosion and mechanical effect.	[109]

Table 2. *Cont.*

Process	Coating	Substrate	Test Method	Main Findings	Ref.
HVOF	Nanostructured Ni–20Cr	SAE213-T22 (T22) and SA 516-Grade 70 steels	Erosion corrosion test (boiler environment)	The investigated nanostructured coating was found to perform better than its conventional (micron-sized Ni–20Cr powder coating) micron-sized counterpart in boiler environment. Nanostructured coating offered better erosion–corrosion resistance under actual boiler conditions, which might be attributed to the presence of protective NiO and Cr_2O_3 phases in their oxide scales and its superior as-sprayed microhardness. Cyclic formation and erosion of the oxide scale occurred during erosion–corrosion phenomenon for coated samples, whereas SA 516 steel was most likely eroded.	[20]
HVOF	Cr_3C_2–25NiCr	310S boiler steel	Cyclic oxidation test	The parabolic rate constant value was one-third for the coated specimen during oxidation as compared to uncoated specimen, which indicates that coating shows better oxidation resistance. The splat and globular morphology of coatings responsible for high degradation resistance of the coatings.	[73]
HVOF AC HVAF	FeCrMoMnWBCSi amorphous	316L SS substrate.	Erosion corrosion test Static electrochemical measurements	AC-HVAF Fe-based amorphous metallic coating exhibits a relatively denser microstructure with high hard phase particles, low porosity, much lower oxide content, and high microhardness compared to HVOF AMC. The AC-HVAF amorphous metallic coating exhibits a higher ability to withstand uniform corrosion and enhanced pitting resistance. The enhanced erosion–corrosion resistance of the AC-HVAF AMC relative to the HVOFAMC could mainly be related to the high hardness and compact structure.	[112]
HVOF	Cr_3C_2–20NiCr	Carbon steel	Wear test Electrochemical corrosion test	The dense surface layer of Cr_3C_2–20NiCr coating have higher corrosion resistance than carbon steel during testing for 27 days. The carbon steel corroded, and iron oxides were present on the surface. Both polarization and EIS results showed the better corrosion protection properties of the coating. Hardness and tribological properties of the coated sample are more durable and the rate of weight loss is very limited compared to substrate material	[103]
HVOF	Cr_3C_2–25NiCr	AISI 304 stainless steel	Tribocorrosion test Electrochemical analysis	No crack or open pores in the HVOF Cr_3C_2–25NiCr coating results in better corrosion resistance against AISI 304 even in the presence of wear. Coefficient of friction (COF) value changes from 0.28 in cathodic conditions to 0.11 in anodic conditions during the test which can be related to the different composition of the sample surface and also passivation film might be present in anodic conditions.	[104]
HVOF Plasma spray	Cr_3C_2–25NiCr	S45C carbon steel	Electrochemical corrosion test	The electrochemical polarization and EIS results indicated that the HVOF coating has superior corrosion resistance to the plasma coating as well as substrate. Less hole formation due to pitting and crevice on the top of HVOF coated samples were responsible for the superior property against plasma spray.	[77,85]
HVOF	Conventional WC–12Co Nanostructured WC–12Co CeO_2-modified WC–12Co	AISI 304 stainless steel	Erosion corrosion test	CeO_2-modified WC–12Co coating possessed the best erosion–corrosion resistance among the other coatings. Conventional WC–12Co coatings have lowest erosion–corrosion resistance. Formation of microcracks in the Co binder phase and generation of corrosion pits, with propagation of the microcracks over the WC particles to expand forward until arriving at the coating surface or a deeper position. This phenomenon causes WC particle falling off from the coating and revealed the failure mechanism of the CeO_2 modified WC–12Co coating.	[21]

Table 2. *Cont.*

Process	Coating	Substrate	Test Method	Main Findings	Ref.
HVOF	WC–CoCr Cr_3C_2–NiCr Al_2O_3	S355 steel	Dry erosion test Slurry erosion test	WC–CoCr coating experienced 5 times higher volume loss under dry erosion compared to slurry erosion due to squeeze film effects. Due to high volume loss in all conditions, Cr_3C_2–NiCr is not a suitable choice to offer increased erosion resistance in dry and slurry environments. WC–CoCr showed a significant reduction in volume loss and wear scar depth over Cr_3C_2–NiCr and Al_2O_3 under both dry jet and slurry erosion results in high hardness.	[81]
HVOF	70Ni30Cr	Martensitic stainless-steel SS 410	Slurry erosion test	The HVOF 70Ni30Cr-coated specimens showed the better combined slurry and cavitation resistance as compared to un coated specimens with 200 µm and 300 µm size sand particle. However, it observed an increase in weight loss with increase in sand particle size and duration of the test.	[113]
HVOF	Cr_3C_2–25NiCr	GH738 Ni-based super alloy	Erosion test	The erosion test results indicate that the volume erosion rate of the coating in addition to, number and depth of the pits on the coating increases with the increase in the air pressure. Above 120 µm coating thickness, the wear rate has negligible variation in the erosion rate. Coating shows better erosion resistance at 90° impact angle as compared to 30° impact angle. Combined behavior of ductile and brittle is the responsible for erosion mechanism of Cr_3C_2–NiCr samples in which ductile mode of erosion characteristic dominates.	[106]
Plasma spray	Ni3Al + Ni–22Cr–10Al–1Y	Superni 75, Superni 600, Superni 718 Superfer 800 H	Erosion corrosion test (boiler environment)	Erosion–corrosion test results in the boiler environment showed that Ni3Al coating layer gets partially oxidized and acts as a perfect barrier against erosion–corrosion of super alloys. Further the partially oxidized coatings remain intact even after 1000 h cycle exposure; thus, it can be presumed that it will enhance the life of boiler tube in the evaluated environment.	[52]
HVAF HVOF	86WC–10Cr–4Co	SS410	Silt erosion test	HVAF WC–CoCr coating at high velocity revealed superior erosion resistance compared to HVAF coating. It could be attributed to the better adhesion, higher density, hardness, and low oxidation, which enhanced erosion resistance of these samples. The erosion wear mechanism observed to be micro-cutting and plowing at lower impact angle. A low cycle fatigue linked to repeated impact leading to rounding of the edges of the WC grains and promote brittle cracking at higher impact angle. Ductile mode of material removal during erosion was indicated by the Erosion Classification Value E_{cv} of the coatings.	[84]
Laser cladding Detonation spraying Plasma spraying	Chromium carbide-NiCrMoNb powder	Steel with 0.27% carbon	Erosion test Nano impact test	Detonation sprayed coating had the lowest erosion rate followed by laser clad coating. Due to brittle nature and poor splat bonding of plasma sprayed coating showed the highest erosion rate. Both dispersion strengthening and solid solution strengthening are found to be effective in enhancing the hardness of Chromium carbide-Ni-rich alloy system. However, excessive dissolution of carbide leads to embrittlement of the Ni rich matrix.	[53]
HVOF	WC−12Co WC−10Co−4Cr Cr_3C_2–25NiCr	316 stainless steel	Wear test Solid particle erosion test Abrasive wear test	Change in erosion mechanism from plastic deformation and micro fracture of carbides to carbide pull out, splat exfoliation, subsurface splat removal, and subsurface cracking occurs due to the transition in erosion rate. The abrasive wear rates of the coatings changes from a mild oxidational wear regime at a load of 20 N to severe wear regime at a load of 40 N. Formation of tribo films and its composition influenced the frictional behavior of the coatings.	[41]

Table 2. *Cont.*

Process	Coating	Substrate	Test Method	Main Findings	Ref.
HVOF	WC–10Co–4Cr	1Cr18Ni9Ti stainless steel	Slurry erosion test Microbial corrosion electrochemical measurement Electrochemical Impedance Spectroscopy (EIS) and Potentiodynamic polarization test	WC–10Co–4Cr coating exhibited a superior slurry erosion–corrosion resistance compared to the substrate material in both distilled water and 3.5 wt. % NaCl slurries. Slurry erosion mechanism in distilled water through formation of cracks and microchipping, whereas in 3.5 wt. % NaCl slurry detachment of binder phase of the coating, microchipping and fragments present in the slurry. Potentiodynamic polarization and EIS results revealed that WC–10Co–4Cr coating had a comparable microbial influenced corrosion resistance in seawater with SRB compared to substrate.	[15]
Thermo-reactive deposition	Cr_7C_3	Medium carbon steel	Erosion corrosion test Potentiodynamic polarization test	No significant dependency to impact angle variation in polarization curves and due to high chemical stability of the Cr_7C_3, there is a slight difference between coated and uncoated samples. However, uncoated sample corrosion potential decreases with increasing impact angle. Cracking and chipping off is the dominant failure mechanism at low impact angle, flake fragmentation, and platelet formation are the main one at 60° for the coated samples.	[54]
HVOF	Cr_3C_2–25NiCr	Carbon steel	Impact test	No adhesive failure was observed under the given test conditions excluding under a loading force of F = 1000 N. Generation of small crater volumes due to plastic deformation, tribo-reaction, and micro-abrasion under impact loading. At critical load conditions with higher forces, induced crack initiation and growth addition to increases the generated crater volume rapidly and the applied force has a decisive influence on the possible failure modes and mechanism. The compressive residual stresses in the HVOF-sprayed coating were important to delay the crack initiation and growth because the effective tensile stresses were reduced during the test.	[54]
HVOF	WC–12Co WC–12Co–10Al_2O_3 WC–12Co–15Al_2O_3	304 stainless Steel	Wear test Potentiodynamic polarization and EIS test	The addition of Al_2O_3 in WC–Co coating enhanced its microhardness and wear properties decrease the wear rate. It is observed that all the coatings showed higher I_{corr} values than substrate which indicates that HVOF coatings have poor corrosion resistance and this is due to the porous nature of the coatings. Thus, it is inferred that the hardness, wear rate, and COF values of the developed WC–12Co–Al_2O_3 HVOF coatings are comparable with hard chrome coating.	[85]
HVOF	Cr_3C_2–25NiCr Cr_3C_2–WC–NiCoCrMo	Plain carbon steel	High temperature wear test	The Cr_3C_2–WC–NiCoCrMo coating exhibits lower porosity and higher hardness compared to the Cr_3C_2–NiCr coating. The Cr_3C_2–WC–NiCoCrMo coating produces relatively higher friction coefficients (COF) compared to the Cr_3C_2–NiCr coating at high temperatures (450, 550, 650 °C) in this testing conditions. Cr_3C_2–WC–NiCoCrMo coatings showed lower wear rates and increased by nearly two times when the temperature increased from 450 to 650 °C, but the wear rates of the Cr_3C_2–NiCr coating are roughly the same, indicating that the microstructure and properties of the Cr_3C_2–WC–NiCoCrMo coating are prone to affect at higher temperature (550–650 °C) compared to the Cr_3C_2–NiCr coating.	[83]
HVOF	Nanostructured WC–10Co4Cr (200–500 nm) Conventional Cr_3C_2–25NiCr NiCrWSiFeB	AISI 1020 steel	Slurry erosion test	Nanostructure coating showed low erosion wear compared to conventional coatings due to higher microhardness value, lower porosity, higher fracture toughness, and lower roughness. Improvements in properties are related to size of the powder particles, density of the coating, and more uniform reinforcement carbides (WC) distribution.	[19]

Table 2. *Cont.*

Process	Coating	Substrate	Test Method	Main Findings	Ref.
HVOF	Conventional Cr_3C_2–25NiCr Nanostructured Cr_3C_2–25NiCr	AISI 1045 steel	Tribo-corrosion tests	Electrochemical data suggested that the corrosion rate of chromium coatings is increased compared to nanostructured coating by almost one order of magnitude by the mechanical damage. The use of nano-sized powders improves the good behavior of the coating due to decrease of the interconnected porosity, a lower roughness, and a better distribution of the chromium carbides in the metal matrix.	[6]
HVOF	Nanostructured WC–Co Conventional WC–Co	UNS G41350 steel	Wear test Potentiodynamic polarization and EIS test	The friction coefficient of the nanostructured WC–Co coating was 30% lower than that of the conventional coating and the wear path was also thinner. The nanostructured coating showed better sliding wear behavior and the higher microhardness seems to be the factor controlling the sliding wear resistance. Nanostructured coating showed a 3.5 times higher corrosion protection due to sealing properties of the coating.	[18]
HVOF	Near-nanocrystalline WC–17Co Microcrystalline WC–Co	AISI 1018 steel	Erosion corrosion test Potentiodynamic polarization test	Near-nanocrystalline coating showed approximately 1/3 lower erosion–corrosion rate than that of the microcrystalline coating and the erosion–corrosion mechanism in the coating was dominated by pure erosion in the microcrystalline coating and the corrosion-enhanced erosion in the near-nanocrystalline coating.	[114]

Peat et al. [81] and Zhou et al. [83] reported that Cr_3C_2–NiCr coating produced the highest volume loss in dry and slurry erosion conditions compared to WC–CoCr and Cr_3C_2–WC–NiCoCrMo coatings due to lower porosity and higher hardness, which has shown better wear resistance and high friction coefficient. Nevertheless, electrochemical measurements in addition to combined erosion–corrosion measurements showed that Cr_3C_2–NiCr coatings were superior with respect to corrosion resistance as compared to WC–Co, WC–NiCrCo, and hard chromium coating under lower erosive conditions as well as WC–Ni coating under low and high erosive conditions, due to fine grain structure and homogeneous distribution of the skeletal network of hard carbide particles within a ductile and corrosion resistant metallic binder. Ni–Cr matrix allows for easier and faster re-passivation with respect to a cobalt one, even when coating is subjected to wear. The corrosion and erosion properties of the cermet-sprayed coatings are not only dependent on the microstructure alone, but the chemical compositions of the matrix, the amount and the size of the carbide particles, and the phase transformations during the deposition are some of the additional factors [87,89,110,111]. Erosion damage parameter and severity of contact can be useful indicators of transition in failure modes. The failure mode and erosion mechanisms were influenced by microstructure of the coatings and the test conditions involving the removal of the carbide grains during the impact together with the corrosion of the binder seems to be insignificant; however, in the second case, the binder erodes inducing a loss of carbide grains after pronounced erosion [41,111]. A few nano and conventional coatings produced by sputtering technique, such as Cr/CrN multilayer, Ti-Si-C-N, CrSiN, as well as HVOF-sprayed Ni–Cr–Si–B–C, plasma-sprayed Ni_3Al + Ni-22Cr-10Al-1Y, laser cladding Cr_3C_2-NiCrMoNb, and thermal reactive deposition Cr_7C_3 coatings showed better erosion–corrosion resistance similar to Cr_3C_2–25NiCr coating over the substrate material at various conditions [47–54].

The role of grain boundaries plays a major role in nanocrystalline Co–Cr Coatings on corrosion. The decrease in the compositional difference between the grain interior and the grain boundary will result in a decrease in the difference between their equilibrium potentials, leading to a low corrosion rate and a uniform corrosion pattern [115]. In addition to the presence of residual strain due to ball milling, intergranular dissolution and high relative grain-boundary-related volume of nanocrystalline materials dramatically influences the repassivation kinetics during corrosion [115]. Nanostructured coating has provided 3.5 times higher protection of the substrate from corrosion due to its nobler behavior and enhanced sealing properties, which is attributed to its lower porosity than that of conventional coating. The nanostructured WC–Co coating showed better sliding wear behavior and the higher microhardness but friction coefficient was 30% lower than that of the conventional coating [18]. Furthermore, nanocrystalline coatings enhance the high-temperature oxidation and corrosion resistance [116].

The erosion–corrosion mechanism of microcrystalline WC-Co coating was dominated by pure erosion whereas the corrosion-enhanced erosion in near-nanocrystalline coating was due to the presence of WC reinforcement at the near-nanocrystalline coating surface. During the erosion process, the vacant site exposed the Co binder surface, which suffered from direct corrosion and this led to a higher erosion–corrosion rate at this site in addition to increased surface roughness compared to nano and near-nano WC-Co coating, attributed to the loss of the larger WC particles from the coating due to the erosive–corrosive action [21,114]. The time dependence of corrosion potential of coated and uncoated steel substrate upon fluid flow with abrasive sand in 3.5 wt. % NaCl + 1000 ppm (~0.001 wt. %) $NaHCO_3$ solution is shown in Figure 8. Near-nanocrystalline coating shows the great positive potential shift (−0.42 V saturated calomel electrode (SCE) after about 9 ks in the test) compared to conventional coating and substrate suggested that protection provided by the near-nanocrystalline coating was higher and more stable than the traditional microcrystalline WC–17Co coating (Figure 8a). Smallest corrosion current density of near nanocrystalline coating confirmed the higher protection. Observed corrosion current density of the near-nanocrystalline coating is smaller than that for conventional coating (Figure 8b). Electrochemical impedance measurements (Nyquist and Bode plots) using open circuit potential for a 4 h test in sand containing solution flowing at a speed of 3 $m{\cdot}s^{-1}$ clearly shows that

the diameter of the capacitive semicircle, which represents the charge transfer resistance in corrosion, was much larger for the near-nanocrystalline coating than the microcrystalline coating, which indicates a decrease in corrosion rate and better protection provided by the near-nanocrystalline WC-17Co coating (Figure 9) [114].

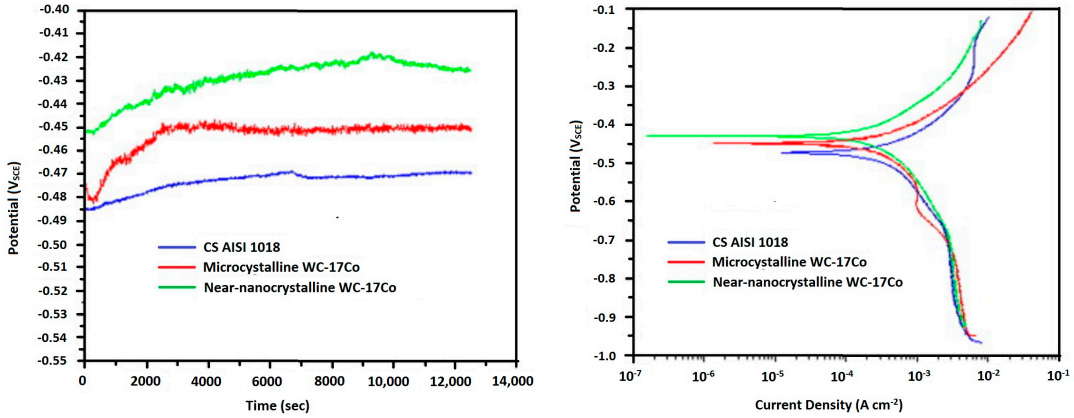

(**a**) (**b**)

Figure 8. Time dependence of corrosion potential (**a**) and Potentiodynamic polarization curves (**b**) for WC–17Co coated and uncoated steel exposed to fluid flow sand particles in 3.5 wt. % NaCl + 1000 ppm (~0.001 wt. %) $NaHCO_3$ solution [114]. Reprinted with permission from ref [114]. © 2011 Elsevier.

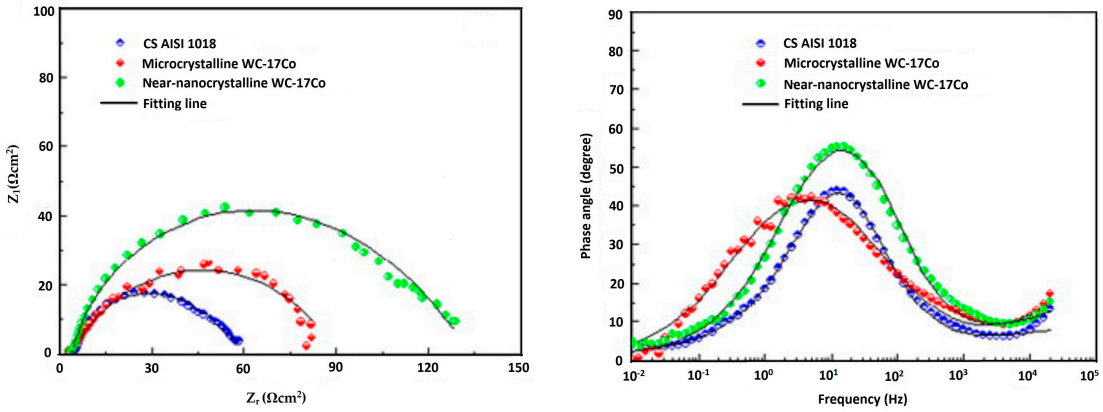

(a) **(b)**

Figure 9. Electrochemical impedance spectroscopy (EIS) of near-nanocrystalline WC–17Co, microcrystalline WC–17Co coatings, and uncoated steel exposed to fluid flow (sand particles in 3.5 wt. % NaCl with 1000 ppm (~0.001 wt. %) $NaHCO_3$ solution): (**a**) Nyquist diagrams and (**b**) Bode plots [114]. Reprinted with permission from ref [114]. © 2011 Elsevier.

Nanostructured Ni-Cr coating offered better erosion–corrosion (E–C) resistance under actual boiler conditions due to the presence of protective NiO and Cr_2O_3 phases in their oxide scales and its superior as-sprayed microhardness. However, in conventional Ni-Cr coating, it was observed that there was an increase in weight loss with increase in sand particle size and duration of the test showed good cavitation erosion resistance [20,113]. Nanostructured WC-based and Cr_3C_2-25NiCr coating showed low erosion–corrosion and erosion-wear compared to conventional coatings corresponding to highest microhardness value, lower porosity, higher fracture toughness, and lower roughness [6,19,21]. The nano carbide ceramic phase mainly causes wear resistance while the corrosion resistance is provided by the binder phase NiCr matrix of the nanostructured Cr_3C_2-25NiCr cermet coatings [73,83,103]. Erosion–corrosion behavior of the nanostructured coatings compared to other conventional coatings mentioned in Table 2 are related to nano-size powder particles, stronger grain strengthening effect,

the density of the coating, binder phase, chemical composition, and the more uniform distribution of reinforcement carbides.

The erosion–corrosion behavior of a WC/Co–Cr coating and mild steel substrate was evaluated with the erodent particles in the slurry (silica sand of size 50 μm mixed in synthetic seawater) prepared according to ASTM D 1141-98 as electrolyte and pH was maintained at 8.2 ± 0.1 and the concentration of particles was 6% by mass [49]. The impact velocity was set at three different values, namely 2, 3, and 4 $m{\cdot}s^{-1}$ and the impact angle was set at 90° [49]. The erosion-corrosion mass losses are significantly lower for the WC/Co–Cr coating compared with the substrate. WC/Co–Cr coating shows that the synergistic effects are at a maximum at the highest potential, however, between 200 to 350 mV (intermediate values), it is surprising that there is a negative synergistic (antagonistic) effect observed and it may be due to the formation of an unstable film, at intermediate potential ranges, which provides some erosion resistance. For the mild steel substrate, there is no evidence of negative synergism. However, the medium synergism regime dominates until high potential values. It is clear that the synergistic regime commences when the anodic corrosion processes occur at higher potential values. This synergistic effect, the effect of corrosion on mechanical wear, may be due to pitting in the presence of chloride ions, making the surface more vulnerable to erosive attack [49].

Stack et al. [49] varied the particle concentration of the slurry at three values 4%, 6%, and 8% (by mass %) in synthetic seawater as an electrolyte with a pH value of 8, and at two impact velocities, namely 2 and 4 $m{\cdot}s^{-1}$ to evaluate the erosion–corrosion resistance of WC/Co–Cr coatings. The slurry was composed of silica sand, with a size in the range 50–250 m. At low velocities (2 $m{\cdot}s^{-1}$), in cathodic conditions, both the coating and the mild steel are favored under the conditions tested. However, at higher potentials, there is a change in performance with the coating favored in preference to the steel, which is due to the significantly lower wastage rates experienced by the coatings, and this is also observed at higher velocities [117]. Erosion–corrosion-resistant behavior of a near-nanocrystalline 'duplex Co coated' WC–17Co coating produced by HVOF spraying was compared with a microcrystalline WC–17Co coating and an uncoated AISI 1018 carbon steel exposed to aqueous solution of 3.5 wt. % sodium chloride (NaCl) + 1000 ppm in weight percent (0.001 wt. %) bicarbonate (HCO_3) as sodium bicarbonate ($NaHCO_3$), and a pH value of 8. The study has shown that the combined erosion–corrosion resistance of the coated coatings was significantly higher than that of the uncoated steel and approximately one-third lower erosion–corrosion rate than that of the microcrystalline coatings [114].

5. Conclusions

Nanostructured coatings sprayed via thermal spray technique have many advantages over conventional coatings and these coatings also carry some excellent properties of great industrial importance. One of the most interesting features of mechanical alloying is understood, which is the ability to produce nanostructure powders and intermetallic compounds. Also, it has been observed that the crystallite size decreases (with increased internal micro-strain) as milling time is increased. At the beginning of milling, amorphous phases were produced but further increment in milling time (12 h) led to increased imperfections and temperature causing crystallization of such phases. Further, the high-energy milling (HEM) powders utilized by HVOF show fine crystalline microstructure with a uniform distribution of small-sized hard phases, which is the reason for low porosity in developed coatings with high micro-hardness/wear resistance. It has been observed that thermal-sprayed coatings utilizing fine feedstock powder provides slightly more wear-resistant coatings than that of a coarse one. It is due to their stronger matrix-carbide cohesion, decreased interconnected porosity, lower roughness, and a better distribution of the chromium carbides in the metal matrix. It is also noted that post-sprayed treatment can significantly influence mechanical and physical properties of these coatings. From the tribo-corrosion study through electrochemical and weight loss measurements, both mechanical and chemical effects were understood, and weight loss measurements clearly showed a synergistic effect due to the combined wear and corrosion degradation. The nanostructured Cr_3C_2-NiCr coatings have

better resistance to individual, as well as combined, effects of erosion and corrosion compared to conventional Cr_3C_2-NiCr coatings.

Although nanostructured cermet coatings have strong technological potential, their applications are limited (wear resistance: Sliding, abrasion, or erosion) to some extent due to expensive processing of nano feedstock powders. Thus, some major improvements are required to utilize the full potential of such nanostructured cermet coatings.

Corrosion resistance enhancement of cermet coatings may also be done by carbide alloying. Potential improvements to selected mechanical and tribological properties of these cermets may be investigated through addition of graphene nano-platelets (GNPs) to a baseline cermet system. The effects of thermal spraying process parameters and post-heat treatment on anticorrosion behavior still need to be studied for these types of coatings. Post-spraying laser surface treatment is advised to produce a crack- and porosity-free layer and improve the corrosion resistance in the case of nanocrystalline cermet coatings. The possibility of introducing new binders with a smaller potential gap with respect to the matrix of the cermet coating may improve the corrosion resistance. Recent advancement in self-sensing corrosion resistant thermal spay cermet coatings based on embedded fiber optic sensors is a technological breakthrough, but high inflight particle speed during HVOF may damage such a sensor and limit potential use of such coatings. The greatest challenges in this field are the lowering of the price of the feedstock powders, increase in the amount of the retained carbides after coating deposition, and the improvement of the mechanical properties of the coatings under elevated temperatures. One of the biggest research gaps seems to be the change of the mechanical properties of cermet coatings during a prolonged time period. The properties of the thermal sprayed cermet coatings, working under elevated temperatures, may improve over time. The carbides oxidize and dissolve in the metal matrix during spraying, therefore the carbide content in the coating is lower than in the feedstock powder. The lower the amount of carbides in the coating, the lower its mechanical properties are; therefore, there are efforts made to increase their content in cermet coatings.

Author Contributions: A.T. and R.J. conceived the idea to write this review paper; A.T., S.S., and G.S. wrote the manuscript; R.J. directed the research and wrote the manuscript and provided useful insights into the manuscript.

Funding: This research was funded by Central Power Research Institute (project sanction number: CPRI/R&D/GEN/2016).

Acknowledgments: The authors would like to thank Central Power Research Institute, Bangalore, India for the financial support provided to execute this work.

Conflicts of Interest: The authors declare no conflict of interest.

References

1. Kumar, H.; Chittosiya, C.; Shukla, V.N. HVOF Sprayed WC Based Cermet Coating for Mitigation of Cavitation, Erosion & Abrasion in Hydro Turbine Blade. *Mater. Today Proc.* **2018**, *5*, 6413–6420. [CrossRef]
2. Rayes, M.M.E.; Abdo, H.S.; Khalil, K.A. Erosion—Corrosion of Cermet Coating. *Int. J. Electrochem. Sci.* **2013**, *8*, 1117–1137.
3. Prasanna, N.D.; Siddaraju, C.; Shetty, G.; Ramesh, M.R.; Reddy, M. Studies on the role of HVOF coatings to combat erosion in turbine alloys. *Mater. Today Proc.* **2018**, *5*, 3130–3136. [CrossRef]
4. Singh Raman, R.K.; Tiwari, A. Graphene: The Thinnest Known Coating for Corrosion Protection. *JOM* **2014**, *66*, 637–642. [CrossRef]
5. Dumée, L.F.; He, L.; Wang, Z.; Sheath, P.; Xiong, J.; Feng, C.; Tan, M.Y.; She, F.; Duke, M.; Gray, S.; et al. Growth of nano-textured graphene coatings across highly porous stainless steel supports towards corrosion resistant coatings. *Carbon* **2015**, *87*, 395–408. [CrossRef]
6. Fedrizzi, L.; Rossi, S.; Cristel, R.; Bonora, P.L. Corrosion and wear behaviour of HVOF cermet coatings used to replace hard chromium. *Electrochim. Acta* **2004**, *49*, 2803–2814. [CrossRef]
7. Mann, B.S.; Arya, V. Abrasive and erosive wear characteristics of plasma nitriding and HVOF coatings: Their application in hydro turbines. *Wear* **2001**, *249*, 354–360. [CrossRef]

8. Hazra, S.; Sabiruddin, K.; Bandyopadhyay, P.P. Plasma and HVOF sprayed WC–Co coatings as hard chrome replacement solution. *Surf. Eng.* **2012**, *28*, 37–43. [CrossRef]
9. Shukla, V.; Jayaganthan, R.; Tewari, V. Degradation behaviour and microstructural characterisation of HVOF-sprayed Cr_3C_2-NiCr cermet coatings in molten salt environment. *Int. J. Mater. Prod. Technol.* **2016**, *53*, 15–27. [CrossRef]
10. Kamal, S.; Sharma, K.V.; Jayaganthan, R.; Prakash, S. Hot corrosion behavior of thermal spray coatings on superalloy in coal-fired boiler environment. *J. Mater. Res.* **2015**, *30*, 2829–2843. [CrossRef]
11. Rana, N.; Mahapatra, M.M.; Jayaganthan, R.; Prakash, S. Deposition of nanocrystalline coatings by modified LVOF thermal spray method. *J. Alloys Compd.* **2014**, *615*, 779–783. [CrossRef]
12. Chen, H.; Si, Y.Q.; McCartney, D.G. An analytical approach to the β-phase coarsening behaviour in a thermally sprayed CoNiCrAlY bond coat alloy. *J. Alloys Compd.* **2017**, *704*, 359–365. [CrossRef]
13. Rana, N.; Mahapatra, M.M.; Jayaganthan, R.; Prakash, S. High-Temperature Oxidation and Hot Corrosion Studies on NiCrAlY Coatings Deposited by Flame-Spray Technique. *J. Therm. Spray Technol.* **2015**, *24*, 769–777. [CrossRef]
14. Rana, N.; Jayaganthan, R.; Prakash, S. Microstructural Features and Oxidation Behaviour of NiCrAlY Coatings Obtained by HVOF Process. *Adv. Mater. Res.* **2012**, *585*, 507–511. [CrossRef]
15. Hong, S.; Wu, Y.; Gao, W.; Zhang, J.; Zheng, Y.; Zheng, Y. Slurry erosion-corrosion resistance and microbial corrosion electrochemical characteristics of HVOF sprayed WC-10Co-4Cr coating for offshore hydraulic machinery. *Int. J. Refract. Met. Hard Mater.* **2018**, *74*, 7–13. [CrossRef]
16. Parida, M.; Nanda, S.P.; Bhuyan, S.K.; Mishra, S.C. Sea water Corrosion of Nickel based Plasma Spray Coating. *Iop Conf. Ser. Mater. Sci. Eng.* **2018**, *338*, 012051. [CrossRef]
17. Bobzin, K.; Zhao, L.; Öte, M.; Königstein, T.; Steeger, M. Impact wear of an HVOF-sprayed Cr_3C_2-NiCr coating. *Int. J. Refract. Met. Hard Mater.* **2018**, *70*, 191–196. [CrossRef]
18. Guilemany, J.; Dosta, S.; Nin, J.; Miguel, J. Study of the properties of WC-Co nanostructured coatings sprayed by high-velocity oxyfuel. *J. Therm. Spray Technol.* **2005**, *14*, 405–413.
19. Reyes-Mojena, M.Á.; Sánchez-Orozco, M.; Carvajal-Fals, H.; Sagaró-Zamora, R.; Camello-Lima, C.R. A comparative study on slurry erosion behavior of HVOF sprayed coatings. *DYNA* **2017**, *84*, 239–246. [CrossRef]
20. Kumar, M.; Singh, H.; Singh, N. Fire side erosion–corrosion protection of boiler tubes by nanostructured coatings. *Mater. Corros.* **2015**, *66*, 695–709. [CrossRef]
21. Liu, Y.; Hang, Z.; Chen, H.; Ceng, S.; Gou, G.; Wang, X.; Tu, M.; Wu, X. Erosion–Corrosion Property of CeO_2-Modified HVOF WC-Co Coating. *J. Therm. Spray Technol.* **2016**, *25*, 815–822. [CrossRef]
22. Ang, A.S.M.; Howse, H.; Wade, S.A.; Berndt, C.C. Manufacturing of nickel based cermet coatings by the HVOF process. *Surf. Eng.* **2016**, *32*, 713–724. [CrossRef]
23. Chatha, S.S.; Sidhu, H.S.; Sidhu, B.S. Characterisation and Corrosion-Erosion Behaviour of Carbide based Thermal Spray Coatings. *J. Miner. Mater. Charact. Eng.* **2012**, *11*, 569–586. [CrossRef]
24. Khan, T.I.; Saha, G.; Glenesk, L.B. Nanostructured composite coatings for oil sand's applications. *Surf. Eng.* **2010**, *26*, 540–545. [CrossRef]
25. He, J.; Schoenung, J.M. Nanostructured coatings. *Mater. Sci. Eng. A* **2002**, *336*, 274–319. [CrossRef]
26. Amin, S.; Panchal, H. A Review on Thermal Spray Coating Processes. *Int. J. Curr. Trends Eng. Res.* **2016**, *2*, 556–563.
27. Stein, K.J.; Schorr, B.S.; Marder, A.R. Erosion of thermal spray MCr–Cr_3C_2 cermet coatings. *Wear* **1999**, *224*, 153–159. [CrossRef]
28. Jacobs, L.; Hyland, M.M.; De Bonte, M. Study of the influence of microstructural properties on the sliding-wear behavior of HVOF and HVAF sprayed WC-cermet coatings. *J. Therm. Spray Technol.* **1999**, *8*, 125–132. [CrossRef]
29. Hawthorne, H.M.; Arsenault, B.; Immarigeon, J.P.; Legoux, J.G.; Parameswaran, V.R. Comparison of slurry and dry erosion behaviour of some HVOF thermal sprayed coatings. *Wear* **1999**, *225–229*, 825–834. [CrossRef]
30. Browning, J. Viewing the future of high-velocity oxyfuel (HVOF) and high-velocity air fuel (HVAF) thermal spraying. *J. Therm. Spray Technol.* **1999**, *8*, 351.
31. Morales, A.T. Coating for Superplastic and Quick Plastic Forming Tool and Process of Using. U.S. Patent US6655181B2, 2 December 2003.

32. Li, C.J.; Wang, Y.Y.; Yang, G.J.; Ohmori, A.; Khor, K.A. Effect of solid carbide particle size on deposition behaviour, microstructure and wear performance of HVOF cermet coatings. *Mater. Sci. Technol.* **2004**, *20*, 1087–1096. [CrossRef]
33. Ji, G.-C.; Li, C.-J.; Wang, Y.-Y.; Li, W.-Y. Microstructural characterization and abrasive wear performance of HVOF sprayed Cr_3C_2–NiCr coating. *Surf. Coat. Technol.* **2006**, *200*, 6749–6757. [CrossRef]
34. Ahmed, R.; Ali, O.; Faisal, N.H.; Al-Anazi, N.M.; Al-Mutairi, S.; Toma, F.L.; Berger, L.M.; Potthoff, A.; Goosen, M.F.A. Sliding wear investigation of suspension sprayed WC–Co nanocomposite coatings. *Wear* **2015**, *322–323*, 133–150. [CrossRef]
35. Pawlowski, L. Suspension and solution thermal spray coatings. *Surf. Coat. Technol.* **2009**, *203*, 2807–2829. [CrossRef]
36. Killinger, A.; Kuhn, M.; Gadow, R. High-Velocity Suspension Flame Spraying (HVSFS), a new approach for spraying nanoparticles with hypersonic speed. *Surf. Coat. Technol.* **2006**, *201*, 1922–1929. [CrossRef]
37. Fauchais, P.; Montavon, G.; Lima, R.S.; Marple, B.R. Engineering a new class of thermal spray nano-based microstructures from agglomerated nanostructured particles, suspensions and solutions: An invited review. *J. Phys. D Appl. Phys.* **2011**, *44*, 093001. [CrossRef]
38. Berghaus, J.O.; Marple, B.; Moreau, C. Suspension plasma spraying of nanostructured WC-12Co coatings. *J. Therm. Spray Technol.* **2006**, *15*, 676–681. [CrossRef]
39. Korpiola, K. *High Temperature Oxidation of Metal, Alloy and Cermet Powders in HVOF Spraying Process*; Helsinki University of Technology: Espoo, Finland, 2004.
40. Ahmed, R.; Faisal, N.H.; Al-Anazi, N.M.; Al-Mutairi, S.; Toma, F.-L.; Berger, L.-M.; Potthoff, A.; Polychroniadis, E.K.; Sall, M.; Chaliampalias, D.; et al. Structure Property Relationship of Suspension Thermally Sprayed WC-Co Nanocomposite Coatings. *J. Therm. Spray Technol.* **2015**, *24*, 357–377. [CrossRef]
41. Vashishtha, N.; Khatirkar, R.K.; Sapate, S.G. Tribological behaviour of HVOF sprayed WC-12Co, WC-10Co-4Cr and Cr_3C_2–25NiCr coatings. *Tribol. Int.* **2017**, *105*, 55–68. [CrossRef]
42. Kear, B.H.; Strutt, P.R. Chemical processing and applications for nanostructured materials. *Nanostructured Mater.* **1995**, *6*, 227–236. [CrossRef]
43. He, J.; Ice, M.; Lavernia, E.J. Synthesis and characterization of nanostructured Cr_3C_2 NiCr. *Nanostruct. Mater.* **1998**, *10*, 1271–1283. [CrossRef]
44. Zhao, Z.; Zheng, H.; Wang, Y.; Mao, S.; Niu, J.; Chen, Y.; Shang, M. Synthesis of chromium carbide (Cr_3C_2) nanopowders by the carbonization of the precursor. *Int. J. Refract. Met. Hard Mater.* **2011**, *29*, 614–617. [CrossRef]
45. Anand, K.; Subramanian, P.R.; Gray, D.M.; Sampath, S.; Huang, S.-C.; Nelson, W.A.; Hasz, W.C. Nano-structured Coating Systems. WIPO Patent Application WO2005056879, 23 June 2005.
46. Tjong, S.C.; Chen, H. Nanocrystalline materials and coatings. *Mater. Sci. Eng. R: Rep.* **2004**, *45*, 1–88. [CrossRef]
47. Bolelli, G.; Berger, L.M.; Börner, T.; Koivuluoto, H.; Matikainen, V.; Lusvarghi, L.; Lyphout, C.; Markocsan, N.; Nylén, P.; Sassatelli, P.; et al. Sliding and abrasive wear behaviour of HVOF- and HVAF-sprayed Cr_3C_2–NiCr hardmetal coatings. *Wear* **2016**, *358–359*, 32–50. [CrossRef]
48. Hodgkiess, T.; Neville, A.; Shrestha, S. Electrochemical and mechanical interactions during erosion–corrosion of a high-velocity oxy-fuel coating and a stainless steel. *Wear* **1999**, *233–235*, 623–634. [CrossRef]
49. Stack, M.M.; Abd El Badia, T.M. Mapping erosion–corrosion of WC/Co–Cr based composite coatings: Particle velocity and applied potential effects. *Surf. Coat. Technol.* **2006**, *201*, 1335–1347. [CrossRef]
50. Alegría-Ortega, J.A.; Ocampo-Carmona, L.M.; Suárez-Bustamante, F.A.; Olaya-Flórez, J.J. Erosion–corrosion wear of Cr/CrN multi-layer coating deposited on AISI-304 stainless steel using the unbalanced magnetron (UBM) sputtering system. *Wear* **2012**, *290–291*, 149–153. [CrossRef]
51. Abd El-Rahman, A.M.; Wei, R. Effect of ion bombardment on structural, mechanical, erosion and corrosion properties of Ti–Si–C–N nanocomposite coatings. *Surf. Coat. Technol.* **2014**, *258*, 320–328. [CrossRef]
52. Mishra, S.B.; Chandra, K.; Prakash, S. Studies on erosion-corrosion behaviour of plasma sprayed Ni_3Al coating in a coal-fired thermal power plant environment at 540 °C. *Anti-Corros. Methods Mater.* **2017**, *64*, 540–549. [CrossRef]
53. Venkatesh, L.; Pitchuka, S.B.; Sivakumar, G.; Gundakaram, R.C.; Joshi, S.V.; Samajdar, I. Microstructural response of various chromium carbide based coatings to erosion and nano impact testing. *Wear* **2017**, *386–387*, 72–79. [CrossRef]

54. Hemmati, A.R.; Soltanieh, S.M.; Masoudpanah, S.M. On the Interaction Between Erosion and Corrosion in Chromium Carbide Coating. *J. Bio-Tribo-Corros.* **2018**, *4*, 10. [CrossRef]
55. Liang, X.B.; Cheng, J.B.; Bai, J.Y.; Xu, B.S. Erosion properties of Fe based amorphous/nanocrystalline coatings prepared by wire arc spraying process. *Surf. Eng.* **2013**, *26*, 209–215. [CrossRef]
56. Roy, M.; Pauschitz, A.; Polak, R.; Franek, F. Comparative evaluation of ambient temperature friction behaviour of thermal sprayed Cr_3C_2–25(Ni20Cr) coatings with conventional and nano-crystalline grains. *Tribol. Int.* **2006**, *39*, 29–38. [CrossRef]
57. Pawlowski, L. Finely grained nanometric and submicrometric coatings by thermal spraying: A review. *Surf. Coat. Technol.* **2008**, *202*, 4318–4328. [CrossRef]
58. Yanpin, L.; Junpeng, M.; Weifeng, Y. Aplication of nanotechnology on hydraulic turbine abrasion and erosion. In Proceedings of the 2010 International Conference on Power System Technology, Hangzhou, China, 24–28 October 2010; pp. 1–3.
59. Luo, P.; Strutt, P.R. Thermal chemical synthesis of nanostructured chromium carbide cermets. *Mater. Sci. Eng. A* **1995**, *204*, 181–185. [CrossRef]
60. Strutt, P.R.; Kear, B.H.; Boland, R.F. Thermal Spray Method for the Formation of Nanostructured Coatings. U.S. Patent US6277448B2, 21 August 2001.
61. Tkachivskyi, D.; Juhani, K.; Surženkov, A.; Kulu, P.; Viljus, M.; Traksmaa, R.; Jankauskas, V.; Leišys, R. Production of Thermal Spray Cr_3C_2-Ni Powders by Mechanically Activated Synthesis. *Key Eng. Mater.* **2019**, *799*, 31–36. [CrossRef]
62. Xu, Z. Nanostructured Powder Metal Compact. European Patent EP2750819A4, 20 January 2016.
63. Lavernia, E.J. Method for Thermal Spraying of Nanocrystalline Coatings and Materials for the Same. U.S. Patent 5939146, 17 August 1999.
64. Lima, R.S.; Marple, B.R. Thermal Spray Coatings Engineered from Nanostructured Ceramic Agglomerated Powders for Structural, Thermal Barrier and Biomedical Applications: A Review. *J. Therm. Spray Technol.* **2007**, *16*, 40–63. [CrossRef]
65. Tao, K.; Zhou, X.-L.; Cui, H.; Zhang, J.-S. Oxidation and hot corrosion behaviors of HVAF-sprayed conventional and nanostructured NiCrC coatings. *Trans. Nonferrous Met. Soc. China* **2009**, *19*, 1151–1160. [CrossRef]
66. He, J.; Lavernia, E.J. Precipitation phenomenon in nanostructured Cr_3C_2–NiCr coatings. *Mater. Sci. Eng. A* **2001**, *301*, 69–79. [CrossRef]
67. Gomari, S.; Sharafi, S. Microstructural characterization of nanocrystalline chromium carbides synthesized by high energy ball milling. *J. Alloys Compd.* **2010**, *490*, 26–30. [CrossRef]
68. Bonache, V.; Salvador, M.D.; Fernández, A.; Borrell, A. Fabrication of full density near-nanostructured cemented carbides by combination of VC/Cr_3C_2 addition and consolidation by SPS and HIP technologies. *Int. J. Refract. Met. Hard Mater.* **2011**, *29*, 202–208. [CrossRef]
69. Lampke, T.; Wielage, B.; Pokhmurska, H.; Rupprecht, C.; Schuberth, S.; Drehmann, R.; Schreiber, F. Development of particle-reinforced nanostructured iron-based composite alloys for thermal spraying. *Surf. Coat. Technol.* **2011**, *205*, 3671–3676. [CrossRef]
70. Sharafi, S.; Gomari, S. Effects of milling and subsequent consolidation treatment on the microstructural properties and hardness of the nanocrystalline chromium carbide powders. *Int. J. Refract. Met. Hard Mater.* **2012**, *30*, 57–63. [CrossRef]
71. Zhao, Z.; Zheng, H.; Zhang, S.; Song, W.; Mao, S.; Chen, Y. Effect of reaction time on phase composition and microstructure of chromium carbide nanopowders. *Int. J. Refract. Met. Hard Mater.* **2013**, *41*, 558–562. [CrossRef]
72. Eigen, N.; Gärtner, F.; Klassen, T.; Aust, E.; Bormann, R.; Kreye, H. Microstructures and properties of nanostructured thermal sprayed coatings using high-energy milled cermet powders. *Surf. Coat. Technol.* **2005**, *195*, 344–357. [CrossRef]
73. Shukla, V.N.; Jayaganthan, R.; Tewari, V.K. Degradation Behavior of HVOF-Sprayed Cr_3C_2-25%NiCr Cermet Coatings Exposed to High Temperature Environment. *Mater. Today Proc.* **2015**, *2*, 1805–1813. [CrossRef]
74. He, J.; Ice, M.; Lavernia, E.J. Synthesis and Characterization of Nanocomposite Coatings. In *Nanostructured Films and Coatings*; Chow, G.-M., Ovid'ko, I.A., Tsakalakos, T., Eds.; Springer: Dordrecht, The Netherlands, 2000; pp. 131–148.

75. He, J.; Ice, M.; Schoenung, J.M.; Lavernia, E.J.; Shin, D.H. Thermal stability of nanostructured Cr_3C_2-NiCr coatings. *J. Therm. Spray Technol.* **2001**, *10*, 293–300. [CrossRef]
76. Jellad, A.; Labdi, S.; Malibert, C.; Renou, G. Nanomechanical and nanowear properties of Cr_3C_2 thin films deposited by rf sputtering. *Wear* **2008**, *264*, 893–898. [CrossRef]
77. Jellad, A.; Labdi, S.; Benameur, T. On the hardness and the inherent ductility of chromium carbide nanostructured coatings prepared by RF sputtering. *J. Alloys Compd.* **2009**, *483*, 464–467. [CrossRef]
78. Roy, M.; Pauschitz, A.; Wernisch, J.; Franek, F. The influence of temperature on the wear of Cr_3C_2–25(Ni20Cr) coating—Comparison between nanocrystalline grains and conventional grains. *Wear* **2004**, *257*, 799–811. [CrossRef]
79. Shmyreva, T.P.; Knapp, J.; Kleyman, A.S. Amorphous-Nanocrystalline-Microcrystalline Coatings and Methods of Production Thereof. U.S. Patent US8465602B2, 18 June 2013.
80. Wang, B.Q. Effect of alkali chlorides on erosion-corrosion of cooled mild steel and Cr_3C_2-NiCr coating. *Wear* **1996**, *199*, 268–274. [CrossRef]
81. Peat, T.; Galloway, A.; Toumpis, A.; Harvey, D.; Yang, W.-H. Performance evaluation of HVOF deposited cermet coatings under dry and slurry erosion. *Surf. Coat. Technol.* **2016**, *300*, 118–127. [CrossRef]
82. Kumar, P.; Sidhu, B.S. Characterization and High-Temperature Erosion Behaviour of HVOF Thermal Spray Cermet Coatings. *J. Mater. Eng. Perform.* **2016**, *25*, 250–258. [CrossRef]
83. Zhou, W.; Zhou, K.; Li, Y.; Deng, C.; Zeng, K. High temperature wear performance of HVOF-sprayed Cr_3C_2-WC-NiCoCrMo and Cr_3C_2-NiCr hardmetal coatings. *Appl. Surf. Sci.* **2017**, *416*, 33–44. [CrossRef]
84. Kumar, R.K.; Kamaraj, M.; Seetharamu, S.; Anand Kumar, S. A pragmatic approach and quantitative assessment of silt erosion characteristics of HVOF and HVAF processed WC-CoCr coatings and 16Cr5Ni steel for hydro turbine applications. *Mater. Des.* **2017**, *132*, 79–95. [CrossRef]
85. Chakradhar, R.P.S.; Prasad, G.; Venkateswarlu, K.; Srivastava, M. An Investigation on the Wear and Corrosion Behavior of HVOF-Sprayed WC-12Co-Al_2O_3 Cermet Coating. *J. Mater. Eng. Perform.* **2018**, *27*, 1241–1248. [CrossRef]
86. Bhatia, R.; Singh, H.; Sidhu, B.S. Characterisation of 80% Cr_3C_2-20% (Ni-20cr) Coating and Erosion Behaviour. *Asian J. Eng. Appl. Technol.* **2012**, *1*, 5–12.
87. Espallargas, N.; Berget, J.; Guilemany, J.M.; Benedetti, A.V.; Suegama, P.H. Cr_3C_2–NiCr and WC–Ni thermal spray coatings as alternatives to hard chromium for erosion–corrosion resistance. *Surf. Coat. Technol.* **2008**, *202*, 1405–1417. [CrossRef]
88. Staia, M.H.; Valente, T.; Bartuli, C.; Lewis, D.B.; Constable, C.P.; Roman, A.; Lesage, J.; Chicot, D.; Mesmacque, G. Part II: Tribological performance of Cr_3C_2-25% NiCr reactive plasma sprayed coatings deposited at different pressures. *Surf. Coat. Technol.* **2001**, *146–147*, 563–570. [CrossRef]
89. Fedrizzi, L.; Valentinelli, L.; Rossi, S.; Segna, S. Tribocorrosion behaviour of HVOF cermet coatings. *Corros. Sci.* **2007**, *49*, 2781–2799. [CrossRef]
90. Gariboldi, E.; Rovatti, L.; Lecis, N.; Mondora, L.; Mondora, G.A. Tribological and mechanical behaviour of Cr_3C_2–NiCr thermally sprayed coatings after prolonged aging. *Surf. Coat. Technol.* **2016**, *305*, 83–92. [CrossRef]
91. Istrate, B.; Munteanu, C.; Lupescu, S.; Benchea, M.; Vizureanu, P. Preliminary Microstructural and Microscratch Results of Ni-Cr-Fe and Cr_3C_2-NiCr Coatings on Magnesium Substrate. *Iop Conf. Ser. Mater. Sci. Eng.* **2017**, *209*, 012024. [CrossRef]
92. Skandan, G.; Yao, R.; Kear, B.H.; Qiao, Y.; Liu, L.; Fischer, T.E. Multimodal powders: A new class of feedstock material for thermal spraying of hard coatings. *Scr. Mater.* **2001**, *44*, 1699–1702. [CrossRef]
93. He, J.; Ice, M.; Lavernia, E.J.; Dallek, S. Synthesis of nanostructured WC-12 pct Co coating using mechanical milling and high velocity oxygen fuel thermal spraying. *Metall. Mater. Trans. A* **2000**, *31*, 541–553. [CrossRef]
94. He, J.; Lavernia, E.J.; Liu, Y.; Qiao, Y.; Fischer, T.E. Near-nanostructured WC-18 pct Co coatings with low amounts of non-WC carbide phase: Part I. Synthesis and characterization. *Metall. Mater. Trans. A* **2002**, *33*, 145–157. [CrossRef]
95. Matthews, S.; James, B.; Hyland, M. The Effect of Heat Treatment on the Oxidation Mechanism of Blended Powder Cr_3C_2-NiCr Coatings. *J. Therm. Spray Technol.* **2010**, *19*, 119–127. [CrossRef]
96. Matthews, S.; James, B.; Hyland, M. The role of microstructure in the mechanism of high velocity erosion of Cr_3C_2–NiCr thermal spray coatings: Part 2—Heat treated coatings. *Surf. Coat. Technol.* **2009**, *203*, 1094–1100. [CrossRef]

97. Matthews, S.; James, B.; Hyland, M. The role of microstructure in the mechanism of high velocity erosion of Cr_3C_2–NiCr thermal spray coatings: Part 1—As-sprayed coatings. *Surf. Coat. Technol.* **2009**, *203*, 1086–1093. [CrossRef]
98. Matthews, S.; Hyland, M.; James, B. Microhardness variation in relation to carbide development in heat treated Cr_3C_2–NiCr thermal spray coatings. *Acta Mater.* **2003**, *51*, 4267–4277. [CrossRef]
99. Matthews, S.J.; James, B.J.; Hyland, M.M. Microstructural influence on erosion behaviour of thermal spray coatings. *Mater. Charact.* **2007**, *58*, 59–64. [CrossRef]
100. Matthews, S.; James, B.; Hyland, M. High temperature erosion of Cr_3C_2-NiCr thermal spray coatings—The role of phase microstructure. *Surf. Coat. Technol.* **2009**, *203*, 1144–1153. [CrossRef]
101. Wang, B.Q. Dependence of erosion–corrosion on carbide/metal matrix proportion for HVOF Cr_3C_2–NiCr coatings. *Surf. Eng.* **1998**, *14*, 165–169. [CrossRef]
102. Guilemany, J.M.; Espallargas, N.; Suegama, P.H.; Benedetti, A.V. Comparative study of Cr_3C_2–NiCr coatings obtained by HVOF and hard chromium coatings. *Corros. Sci.* **2006**, *48*, 2998–3013. [CrossRef]
103. Akhtari Zavareh, M.; Sarhan, A.A.D.M.; Razak, B.B.; Basirun, W.J. The tribological and electrochemical behavior of HVOF-sprayed Cr_3C_2–NiCr ceramic coating on carbon steel. *Ceram. Int.* **2015**, *41*, 5387–5396. [CrossRef]
104. Pileggi, R.; Tului, M.; Stocchi, D.; Lionetti, S. Tribo-corrosion behaviour of chromium carbide based coatings deposited by HVOF. *Surf. Coat. Technol.* **2015**, *268*, 247–251. [CrossRef]
105. Akhtari Zavareh, M.; Mohammed Sarhan, A.A.D.; Akhtari Zavareh, P.; Basirun, W.J. Electrochemical corrosion behavior of carbon steel pipes coated with a protective ceramic layer using plasma and HVOF thermal spray techniques for oil and gas. *Ceram. Int.* **2016**, *42*, 3397–3406. [CrossRef]
106. Zhang, H.; Dong, X.; Chen, S. Solid particle erosion-wear behaviour of Cr_3C_2–NiCr coating on Ni-based superalloy. *Adv. Mech. Eng.* **2017**, *9*. [CrossRef]
107. Kumarasamy, M.; Natarajan, S. Selection and characterisation of HVOF cermet coatings for volutes of high capacity pumps of opencast lignite mines. *Surf. Eng.* **2016**, *32*, 229–237. [CrossRef]
108. De Souza, V.A.; Neville, A. Corrosion and erosion damage mechanisms during erosion–corrosion of WC–Co–Cr cermet coatings. *Wear* **2003**, *255*, 146–156. [CrossRef]
109. Hong, S.; Wu, Y.; Zhang, J.; Zheng, Y.; Qin, Y.; Gao, W.; Li, G. Cavitation Erosion Behavior and Mechanism of HVOF Sprayed WC-10Co-4Cr Coating in 3.5 wt% NaCl Solution. *Trans. Indian Inst. Met.* **2015**, *68*, 151–159. [CrossRef]
110. Wang, B.Q.; Luer, K. The erosion-oxidation behavior of HVOF Cr_3C_2-NiCr cermet coating. *Wear* **1994**, *174*, 177–185. [CrossRef]
111. Toma, D.; Brandl, W.; Marginean, G. Wear and corrosion behaviour of thermally sprayed cermet coatings. *Surf. Coat. Technol.* **2001**, *138*, 149–158. [CrossRef]
112. Wang, Y.; Xing, Z.Z.; Luo, Q.; Rahman, A.; Jiao, J.; Qu, S.J.; Zheng, Y.G.; Shen, J. Corrosion and erosion–corrosion behaviour of activated combustion high-velocity air fuel sprayed Fe-based amorphous coatings in chloride-containing solutions. *Corros. Sci.* **2015**, *98*, 339–353. [CrossRef]
113. Amarendra, H.J.; Prathap, M.S.; Karthik, S.; Darshan, B.M.; Devaraj; Girish, P.C.; Runa, V.T. Combined Slurry and Cavitation Erosion Resistance of Hvof Thermal Spray Coated Stainless Steel. *Mater. Today Proc.* **2017**, *4*, 465–470. [CrossRef]
114. Saha, G.C.; Khan, T.I.; Zhang, G.A. Erosion–corrosion resistance of microcrystalline and near-nanocrystalline WC–17Co high velocity oxy-fuel thermal spray coatings. *Corros. Sci.* **2011**, *53*, 2106–2114. [CrossRef]
115. Cheng, D.; Tellkamp, V.L.; Lavernia, C.J.; Lavernia, E.J. Corrosion Properties of Nanocrystalline Co–Cr Coatings. *Ann. Biomed. Eng.* **2001**, *29*, 803–809. [CrossRef]
116. Wang, F.; Geng, S. High Temperature Oxidation and Corrosion Resistant Nanocrystalline Coatings. *Surf. Eng.* **2013**, *19*, 32–36. [CrossRef]
117. Stack, M.M.; Abd El-Badia, T.M. Some comments on mapping the combined effects of slurry concentration, impact velocity and electrochemical potential on the erosion–corrosion of WC/Co–Cr coatings. *Wear* **2008**, *264*, 826–837. [CrossRef]